

## **Distribution Agreement**

In presenting this thesis as a partial fulfillment of the requirements for a degree from Emory University, I hereby grant to Emory University and its agents the non-exclusive license to archive, make accessible, and display my thesis in whole or in part in all forms of media, now or hereafter now, including display on the World Wide Web. I understand that I may select some access restrictions as part of the online submission of this thesis. I retain all ownership rights to the copyright of the thesis. I also retain the right to use in future works (such as articles or books) all or part of this thesis.

Hyunjun Max Ahn

March 24, 2021

Structure and Function of Potassium Chloride Cotransporter KCC3

by

Hyunjun Max Ahn

Bo Liang, PhD.  
Adviser

Neuroscience and Behavioral Biology

Bo Liang, PhD.  
Adviser

Leah Anderson Roesch, PhD.  
Committee Member

Victor Faundez, MD. PhD.  
Committee Member

2021

Structure and Function of Potassium Chloride Cotransporter KCC3

By

Hyunjun Max Ahn

Bo Liang, PhD.

Adviser

An abstract of  
a thesis submitted to the Faculty of Emory College of Arts and Sciences  
of Emory University in partial fulfillment  
of the requirements of the degree of  
Bachelor of Science with Honors

Neuroscience and Behavioral Biology

2021

## Abstract

### Structure and Function of Potassium Chloride Cotransporter KCC3

By Hyunjun Max Ahn

Potassium Chloride Cotransporters (KCC) mediates electroneutral transport of one chloride ion with a potassium ion that is involved in cell volume regulation, salt reabsorption, and maintaining ion concentration across the cell membrane. As important as its physiological functions are, the exact molecular mechanism of this protein has been limited due to the lack of high-resolution 3-D structures of these proteins. To investigate the structure and the function of the protein, cryogenic electron microscopy (cryo-EM) images of the KCC3 proteins were obtained in an attempt to elucidate its structure. Here, we use negative stain and cryogenic electron microscopy to characterize the general molecular shape and the architecture of the protein. We discovered that KCC3 is in dimeric form, comparable to the previously published KCC1 structure. We also demonstrate that the cryo-EM images are much more sensitive to the type of detergents and polymers used to stabilize the membrane protein than the negative stain EM images. Furthermore, we established an optimized transient PEI-based transfection to obtain the higher yield of a membrane protein using suspension HEK293F cells. Overall, this study can serve as a groundwork for the expression and purification of other membrane proteins for structural and functional investigations.

Structure and Function of Potassium Chloride Cotransporter KCC3

By

Hyunjun Max Ahn

Bo Liang, PhD.

Adviser

A thesis submitted to the Faculty of Emory College of Arts and Sciences  
of Emory University in partial fulfillment  
of the requirements of the degree of  
Bachelor of Science with Honors

Neuroscience and Behavioral Biology

2021

## Acknowledgements

I would like to thank Dr. Bo Liang for giving me the opportunity to conduct research in his laboratory. Your mentorship to me over my past four years has been invaluable to me, helping me to develop not only as a better researcher but also as an academic scholar. My undergraduate experience could not have been better without the Liang lab, and through this lab I was able to find my new passion in research that I hope to have it as part of my future careers. Thank you for believing in me, and for your patience and eagerness to help me throughout my undergraduate research. “Good work” that you always say at the end of every meeting was always truly encouraging that has helped me be persistent despite so many obstacles throughout the process.

I would like to thank Dr. Yunrong Gao, my former postdoctoral mentor. Thank you for your compassion, patience, and desire to teach different lab techniques when I first joined the lab as a college first-year student. I really appreciated your inviting smiles, enthusiasm, and humors that brightened my day every time I come into the lab. Thank you also so much for helping me troubleshoot our plasmid purification experiment.

I would also like to thank Dr. Dongdong Cao, another postdoctoral researcher in our research lab. Thank you for your desire to share knowledge and always being there whenever I need something. Thank you so much for always asking if I need anything and offering help. Thank you so much also for providing insights for maintaining the cell culture.

I would like to thank Jasmine Berry, Anna Antonova, and Maurice Terrell Royal for offering advice and helping me maintain the mammalian cell culture. I would like to thank Dr. Qi Wang for helping me with the protein purification.

I would like to thank Dr. Leah Anderson Roesch for her guidance, enthusiasm, optimism, and encouragement throughout the thesis process.

I would like to thank Dr. Victor Faundez for his guidance, enthusiasm, insightful suggestions, and support throughout the thesis process.

## Table of Contents

<b>Introduction</b>	1
Membrane Protein Structural Studies	3
Traditional Detergents	4
Amphipols	5
Nanodiscs	6
Fab	6
Tag designs	7
PEI Transfection	8
<b>Methods</b>	8
Transformation	8
Plasmid Purification	9
N-MBP-PPX-KCC3 Protein Expression Using Baculovirus	10
N-10x His tag-KCC3 Protein Expression Using PEI-based Transfection Method 1	10
N-10x His tag-KCC3 Protein Expression Using PEI-based Transfection Method 2	11
N-MBP-PPX-KCC3 Protein Purification	11
N-10x His tag-KCC3 Protein Purification	12

Nanodisc and Amphipol Reconstitution _____	12
Negative Stain Electron Microscopy Grid Preparation _____	13
Cryo Electron Microscopy Grid Preparation _____	13
<b>Results</b> _____	14
Protein Expression and Purification of N-MBP-PPX-KCC3 _____	14
Negative Stain Images of KCC3 _____	16
Cryo Grid Screening Images of KCC3 _____	18
Cryogenic Electron Microscopy Image Processing _____	23
Transformation and Plasmid purification of N-10x His tag-KCC3 _____	25
PEI-based Transfection _____	26
<b>Two Additional Studies Using Similar Techniques</b> _____	34
Gel Filtration Profile and Negative Stain EM to Characterize the Protein _____	34
High Resolution Structure Involving His-tag Purification and Protease Cleavage _____	40
<b>Discussions</b> _____	41
PEI-based transfection of N-10x his tag-KCC3 _____	41
N-Terminus Purificaiton Tag _____	41
General architecture and electron microscope images of N-MBP-PPX-KCC3b _____	42

<b>Known Structural Insights into KCC Families</b>	44
Structural Analysis of KCC1	44
Structural Analysis of Monomeric KCC4	45
Structural Analysis of Dimeric KCC2, KCC3, and KCC4	46
<b>Conclusions</b>	49
<b>Supplemental Tables</b>	50
Table 1: Table Summary of Purification Tags to Different Membrane Protein for Structural Studies	
Table 2: Table Summary of Buffer Conditions of Different KCC for Cryo-EM studies	
<b>Supplemental Figures</b>	55
Supplemental Figure 1: Proteins Encoded by SLC12 Gene	
Supplemental Figure 2: General Workflow of Cryo-EM Image processing	
Supplemental Figure 3: General Workflow of Membrane Protein Purification	
Supplemental Figure 4: Comparison Between Linear and Conformational Epitope	
Supplemental Figure 5: Carton Representation of Protein in Cryo-EM Grids	
Supplemental Figure 6: Example Image of Particle Picking of Cryo Grid Images	
Supplemental Figure 7: 2D Classifications of KCC3	
Supplemental Figure 8: Gel Electrophoresis Image of the Plasmid	

Supplemental Figure 9: Small Volume Expression Test

Supplemental Figure 10: Small Volume Expression Test After VPA and SB

Supplemental Figure 11: Cryo-EM Images of Potassium-Chloride Cotransporters

Supplemental Figure 12: Ion Binding Sites of KCC4

Supplemental Figure 13: N-terminal Peptide of KCC2

Supplemental Figure 14 : Hydrophobic Interactions Involved in KCC Dimerization

## **Introduction**

Cation-Chloride Cotransporter (CCC) is a transmembrane transporter protein that mediates the coupled, electroneutral symport of chloride, potassium, and/or sodium across the plasma membrane. These proteins are synthesized by the human Solute Carrier 12 (SLC12) gene, and play a vital role in cell volume regulation, salt reabsorption, and maintaining intracellular ion concentration. Depending on the ion being transported across the membrane, CCCs are divided into several branches: Two Na-K-2Cl cotransporters (NKCC1 and NKCC2) encoded by SLC12A1 and SLC12A2; One Na-Cl cotransporter (NCC) encoded by SLC12A3; Four K-Cl cotransporter (KCC1, KCC2, KCC3, and KCC4) encoded by SLC12A4 to SLC12A7 (Supplemental Figure 1.) (Gamba, 2005).

Of all the transporters under the cation-chloride cotransporter family, KCC plays many vital roles in different cell types. All four potassium chloride cotransporters except KCC2 is osmolarity sensitive (Mercado et al., 2006). KCC2 is often one of the most widely studied proteins because its neuronal specificity and its important role keeping the concentration of intracellular chloride low for the GABAergic system of the central nervous system. Of all the KCC, KCC3 is our specific interest being expressed in the white matter of the CNS (Pearson et al., 2001), sensory neurons in PNS (Byun and Delpire, 2007), astrocytes (Walz and Hertz, 1984), neurons (Thompson et al., 1988), choroid plexus (Zeuthen, 1994), heart (Garneau et al., 2016), and kidney (Pearson et al., 2001). It is hypothesized that while KCC2 plays a major role in the CNS, PNS neurons are particularly dependent on the KCC3 proteins, because PNS neurons relatively lack KCC2 proteins (Kahle et al., 2016). KCC3 is activated via tyrosine dephosphorylation in the C-terminus in response to the cell swelling, causing efflux of the water by the symport of chloride and potassium outside the cells (Flores et al., 2019).

Overall, cation-chloride cotransporters play a critical role in human physiology, and mutations in these transporters can lead to many different diseases. For example, it has been characterized that the mutations in R952H and R1049C in SLC12A5 that leads to reduced activity of KCC2 causes idiopathic generalized epilepsy (Kahle et al., 2014), while the loss-of-function mutations in the same gene caused epilepsy of infancy with migrating focal seizures and significant motor deficits (Stodberg et al., 2015). Similarly, it is characterized that the deletion mutation in KCC3 (2436delG, Thr813fsX813) or missense mutation (R207C or R207H) that accompanied loss-of-function (LOF) was linked with Hereditary Motor Sensory Neuropathy related to the agenesis of the corpus callosum with symptoms such as psychosis, mental retardation (Howard et al., 2002; Flores et al., 2019; Uyanik et al., 2006; Park et al., 2019). Similarly, LOF mutation is also linked with Andermann syndrome, characterized by severe sensorimotor neuropathy with areflexia, amyotrophy, and locomotor abnormalities (Bowerman et al., 2017), as well as decreased seizure threshold and progressive deafness from loss of sensory hair cells (Boettger et al., 2003). Interestingly, Kahle and his colleague (2016) described a child with motor neuropathy associated with gain-of-function (GOF) mutation of KCC, which unlike LOF mutation, is characterized with intact corpus callosum and cognitive ability (Kahle et al., 2016).

Since the initial discovery and expression of the potassium chloride (KCC) cotransporter (Mount et al., 1999), there have been many attempts to further identify and characterize this protein. While many biochemical assays and mutational studies were done to elucidate its significance in its pathophysiology and its regulatory roles, much of our understanding on its molecular function has been limited until very recently due to the lack of 3-D structures of the proteins. High resolution structural studies may provide invaluable resources for the researchers to further understand its exact mechanism. They further enable researchers to use the structure to conduct rational drug

design studies, which can be used to develop a new targeting molecule, which could treat disorders associated with the protein by altering its activity.

### **Membrane Protein Structural Studies**

With many breakthroughs in cryo-EM technology, along with the development of new membrane protein solubilizing mechanisms in the past few years, protein structural studies are becoming increasingly popular. Most notably being the major breakthrough of using a direct electron detection camera – previously proteins were imaged through phosphor scintillators, which converted electrons to photons, rather than detecting electrons directly (Liao et al., 2014).

Cryo-EM is advantageous over X-ray crystallography because it requires a fewer amount of proteins (on the order of microgram rather than a milligram). Furthermore, cryo-EM does not require ‘locking’ the proteins in certain conformation, which sometimes may involve additional co-factors, ligands, or toxins to stabilize the proteins into certain conformation (Liao et al., 2014). In fact, cryo-EM allows the detection of different classifications of the proteins in their native state, which allows us to separate different protein conformations.

Many factors rely on obtaining the cryo-EM structure of the membrane protein which includes the production of biochemically stable proteins, use of a well-characterized drug, novel electron detection camera, and ability to separate different classes of heterogeneous protein mixture (Liao et al., 2014), as well as the use of effective solubilization and reconstitution methods for the proteins. Ideally, the samples in the cryo-EM grids must have even distribution and display random orientations in the ice layer without any aggregation, which are often very hard to achieve with little reproducibility (Drulyte et al., 2018).

The general workflow of the Cryo-EM data processing is summarized in Supplemental Figure 2 (Liu et al., 2019). Cryo-EM micrograph includes images of many macromolecule single particles that are in random orientation. The overarching goal of Cryo-EM single particle reconstruction is to superimpose these single particles that are consistent in the conformation that they are able to provide a density map that can be used to determine the molecular structure of the macromolecules (Frank, 2002). In order to achieve the single-particle reconstruction, several classifications and refinement must be done after obtaining the images of the protein particles from the cryo-EM micrograph. First, 2D classification is done to identify the obviously bad and unwanted image, as well as to sort heterogeneous mixture. Then, 3D classification is applied to sort the particles into the distinct homogenous population from the heterogeneous mixture of the particles, as well as to select particles that are suitable for high-resolution reconstruction (Serna, 2019). Lastly, 3D modeling is applied to compare the differences and the similarities between the images obtained from the 3D reconstruction and superimpose the images to reconstruct single particles (Serna, 2019).

### **Traditional Detergents**

Detergents are required to solubilize the membrane proteins from the membrane and also stabilize the membrane proteins in amphiphilic conditions. The concentration of the detergent must be well-optimized because too many detergents may create noise through micelle formation, while too few detergents (lower than critical micelle concentration (CMC)) may cause proteins to dissociate from the detergent and aggregate (Liao et al., 2014). Furthermore, detergents are known to influence the surface tension of water and thickness of the vitreous ice in the cryo-grid that may cause more challenges in the Cryo-EM studies (Liao et al., 2014). Lastly, it is well known that

detergents disturb the protein structures and functions that may hinder the functional and structural study of the proteins (Autzen et al., 2019). Despite many possible challenges and difficulties, many X-ray crystallography and Cryo-EM have been successful in determining membrane protein structures in the detergent such as n-Dodecyl-B-D-Maltoside (DDM), digitonin, Lauryl Maltose Neopentyl Glycol (LMNG), glyco-diosgenin (GDN), and many more (Supplemental Table 2.)

### **Amphipols**

Amphipols are amphipathic polymers with a hydrophilic backbone (Dorr et al., 2016). While they still require traditional detergents to solubilize membrane proteins from the membrane (Supplemental Figure 3.), amphipols can be substituted in the reconstitution step of membrane protein purification experiments (Liao et al., 2014). Compared to traditional detergents, amphipols have a higher affinity towards the hydrophobic transmembrane domain and remain more tightly bound with the membrane protein, even when the concentration is lower (Le Bon et al., 2018).

These characteristics overcome some of the challenges caused by traditional detergents: With amphipols, proteins are less likely to dissociate from the micelles to self-aggregate, and amphipols are less likely to create noise in the cryo-EM images (Liao et al., 2014); they may also bypass the negative influences on the ice thickness and surface tension introduced by the detergents (Liao et al., 2014). Some of the commonly utilized amphipols are A8-35 and PMAL-C8.

### **Nanodisc**

A nanodisc consists of a discoidal lipid bilayer that is stabilized by two membrane scaffold proteins (MSP) encircling a lipid (Liao et al., 2014). Nanodiscs may provide more ideal conditions that more closely resemble the native lipid bilayer environment of the membrane protein than traditional detergents or amphipols (Dorr et al., 2016). This method was developed by the Sligar lab in 2002, and since then, there has been growing popularity in determining the structures using this method (Bayburt et al., 2002). Through this method, it may also be possible to study the lipid-protein interaction (Liao et al., 2014). A further advantage may include that because MSP determines the size of the nanodisc, it may result in more homogeneous protein-nanodisc particles, which facilitates cryo-EM studies (Liao et al., 2014; Autzen et al., 2019).

It should be noted that nanodisc, like amphipols, is used for the reconstitution method and does not bypass the solubilization that is facilitated by the detergents (Liao et al., 2014). One of the new technologies that are recently being developed involves styrene-maleic acid copolymer, which is able to solubilize the membrane protein in its crude membrane without using detergents that may disrupt the membrane protein structure (Dorr et al., 2016).

## **Fab**

Historically, there have been many challenges in obtaining a 3-D high-resolution Cryo-EM structure of the small proteins with molecular weight less than 100 kDa (Wu et al., 2012). This is due to the following reasons: difficulty in the visualization of small proteins in vitreous ice, lack of obvious structural features for image alignment, small fluctuation creating so much noise that can be strongly influenced by the reference model (Wu et al., 2012). There have been many attempts to go around these challenges, and in 2012, Wu et al. have presented the method of using fragment antigen-binding (Fab) protein in an attempt to overcome these challenges.

First, as Fab binds to the target protein, it increases the molecular weight of the target protein for better detection through EM. Furthermore, Fab has a distinct feature characterized by the “hole in the middle and other by two blobs”, which its distinct feature can be used to facilitate image alignment in the Cryo-EM data processing, as well as also determine whether the structural classification is valid (Wu et al., 2012).

In order for Fab-protein complex to work, Fab must form a rigid complex. This means that it must bind to the conformational epitope (as opposed to linear epitope) (Supplemental Figure 4) in a region where it is inflexible (Wu et al., 2012). This is often a very time-consuming process, as various Fab must be generated and analyzed through SEC/negative stain EM for optimization to ensure that the fab binding is specific to the inflexible regions of the protein. It should be noted that the Fab must not be bound to genetically introduced tags in the structural studies, as the linker sequence in between is often flexible.

### **Tag designs**

As noted previously, structural studies of membrane protein require purified microgram quantities of the protein (Liao et al., 2014). Many scientists use affinity chromatography for protein purification, which is summarized in Supplemental Table 1. They include but are not limited to, his-tag, strep tag, flag tag, and MBP tag. It should be noted that while plasmids can be designed so that the tags can be attached to either of the termini, functions of some proteins may be sensitive to which ends of the protein the tag is attached to (Agez et al., 2017).

### **PEI Transfection**

Polyethylenimine (PEI) based transfection is widely used for transient transfection of the plasmid that can introduce DNA into the mammalian cells with lower cost, toxicity, and immunogenicity (Aslan et al., 2006). PEI is a cationic polymer that can form the complex with the DNA to condense it to positively charged particles (Boussif et al., 1995). The positively charged DNA-PEI complex can then be bound to the anionic cell surfaces and the DNA is introduced into the cells via endocytosis (Sonawane et al., 2003; Longo et al., 2013). Currently, there are mainly two established protocols in PEI-based transfection. One method involves introducing DNA into the cell culture first, followed by the addition of the PEI (Subedi et al., 2015). Another method involves the formation of DNA/PEI complex first, followed by the addition of this complex into the cell culture (Portolano et al., 2014). In this study, both methods were tested with varying DNA/PEI ratios with different conditions were tested for optimization of the protein expression.

## **Methods**

In this study, we have expressed the proteins using different constructs of the KCC3b wild type sequence: N-MBP-PPX-Truncated KCC3 (109-1099), N-MBP-PPX-Full length KCC3 (1-1099), N-10x his tag-PPX-Truncated KCC3 (109-1099), and N-10x his tag-PPX-Full length KCC3 (1-1099).

## **Transformation**

Human SLC12A6 gene encoding for 10x his tag-TEV-KCC3b were codon optimized and synthesized by Synbio Technologies. Top 10 *E. coli* competent cells were taken from -80 °C freezer and thawed. The 2uL of the plasmid (100 ng/uL) containing the gene was added to 30 uL of the competent cells. The Top 10 *E. coli* cells were heat-shocked by incubating them in the

following sequence: 30 minutes in ice, 45 seconds in 42 °C water bath, then 2 minutes in ice. Then 500 uL of LB media was added to the cells and incubated in a 37 °C shaker for 1 hour. 50 uL of the cells were plated overnight on the LB agar plate with ampicillin. Colonies were then picked and grown in 500mL LB media for 16 hours and were further split into 2\*1L and 1\*0.5L LB media for overnight

### **Plasmid Purification**

Plasmid containing KCC3b gene purified using the Gigaprep Kit (Qiagen). Cells were harvested at 3800 rpm using the centrifuge. Then, the cells were resuspended using 100 mL P1 buffer (50 mM Tris Cl, pH 8.0, 10 mM EDTA, 100 ug/mL RNase A), lysed by incubating the cells with 100 mL P2 buffer (200 mM NaOH, 1% SDS (w/v)) and at last neutralized using 100 mL S3 buffer (Qiagen). Then, the lysates were loaded onto QIAfilter Cartridge (Qiagen) and were incubated for 10 minutes so the cell debris floats on the top to facilitate the filtering process. The cell lysates were filtered through the Cartridge and eluants containing the plasmids were collected. Then, BB Buffer (Qiagen) was added to adjust the correct binding conditions for the plasmid. Lysates are then transferred to Plasmid Plus Spin column (Qiagen) in the vacuum, and the plasmids were washed using 80 mL ETR (Qiagen) and 50 mL of PE buffer (Qiagen). The spin column was then centrifuged at 4000 x g for 10 mins to dry the column. 3 mL of Buffer EB (10 mM Tris-Cl, pH 8.5) was then added onto the membrane of the column and incubated for 1 min before centrifuging at 4000 x g for 5 mins to collect the plasmid. Then, the same elution step was repeated using 2 mL of Buffer EB.

### **N-MBP-PPX-KCC3 Protein Expression Using Baculovirus**

The full-length and truncated human SLC12A6 gene containing the MBP tag was cloned and expressed in HEK293 cells using the BacMam System. HEK 293 cells were cultured to 1L before transfection in BalanCD (Fujifilm). The baculovirus was generated in Sf9 insect cells and was used to infect HEK293F cells at the ratio of 1:20 (virus: HEK293, v/v). Cells are then supplemented with 20 mM sodium butyrate for KCC3 protein expression after 24 hours and cultured at 30 °C for additional 48 hours. The cell pellets are then centrifuged at 3000 g, washed with PBS buffer (137 mM NaCl, 2.7 mM KCl, 10 mM Na<sub>2</sub>HPO<sub>4</sub>, 1.8 mM KH<sub>2</sub>PO<sub>4</sub>, 1 mM CaCl<sub>2</sub>, 0.5 mM MgCl<sub>2</sub>), then centrifuged again at 3000 g and was stored in -80 °C freezer until purification.

#### **N-10x His tag-KCC3 Protein Expression Using PEI-based Transfection Method 1**

HEK 293F cells were used for transfection. The cell density should be around  $1 \times 10^6$  cells/mL at the time of transfection. The cells were seeded at  $0.5 \times 10^6$  cells/mL 24 hours before the transfection at 37°C incubator. The final transfection volume should be 20-30% of the total volume of the suspension flask. 1 ug DNA/ml cell culture or 1.5 ug DNA/ml cell culture was added to 50% of the final transfection volume and incubated for 5 minutes at 37°C, 8% CO<sub>2</sub>. Then, the PEI was added to the cell culture so that the final ratio of DNA: PEI is in the range of 1:1.5 to 1:5. It was then incubated for 24 hours in 37°C. It was then diluted 1:1 with the cell media supplemented with 3 mM valproic acid for protein expression and incubated for 48 more hours in 30 °C before the cells were harvested for protein purification. The cell pellets are then centrifuged at 3000 g, washed with PBS buffer (137 mM NaCl, 2.7 mM KCl, 10 mM Na<sub>2</sub>HPO<sub>4</sub>, 1.8 mM KH<sub>2</sub>PO<sub>4</sub>, 1 mM CaCl<sub>2</sub>, 0.5 mM MgCl<sub>2</sub>), then centrifuged again at 3000 g and was stored in -80 °C freezer until purification.

### **N-10x His tag-KCC3 Protein Expression Using PEI-based Transfection Method 2**

The cells were seeded at  $0.5 \times 10^6$  cells/mL 24 hours before the transfection at 37°C incubator. HEK293 cell density should be around  $1 \times 10^6$  cells/mL at the time of transfection. The final transfection volume should be 20-30% of the total volume of the suspension flask. Before transfection, DNA and PEI were mixed so that the ratio of DNA: PEI is in the range of 1:1.5 to 1:5 and incubated at room temperature for 20 minutes. They were then added to the cell culture so that the final concentration of DNA is 1 ug DNA/ml cell culture or 1.5 ug DNA/ml cell culture. Cells are then supplemented with 20 mM sodium butyrate or 3 mM Valproic acid for KCC3 protein expression after 3 or 24 hours and cultured at 30 °C or 37°C for additional 48 hours. The cell pellets are then centrifuged at 3000 g, washed with PBS buffer (137 mM NaCl, 2.7 mM KCl, 10 mM Na<sub>2</sub>HPO<sub>4</sub>, 1.8 mM KH<sub>2</sub>PO<sub>4</sub>, 1 mM CaCl<sub>2</sub>, 0.5 mM MgCl<sub>2</sub>), then centrifuged again at 3000 g and was stored in -80 °C freezer until purification.

### **N-MBP-PPX-KCC3 Protein Purification**

Cells were resuspended in lysis buffer (30 mM Tris-HCl pH 8.0 and 150 mM KCl or 150 mM NaCl) with Protease Inhibitor cocktail pills (Sigma-Aldrich). Then, cells were lysed using a Dounce homogenizer. Then, the detergent A (1% LMNG with 0.1% CHS or 1% DDM with 0.1% CHS) is added to the sample and stirred for 3.0 h at 4 C to extract the membrane protein. The samples were ultracentrifuge at 40, 000 rpm for 1 hour to collect the supernatant containing membrane protein. The sample was incubated in maltose beads and was collected in the Bio-Rad gravity column. They are washed using Wash Buffer (30 mM Tris-HCl pH 8.0, 150 mM KCl or 150 mM NaCl, 0.1% DDM/LMNG with 0.1% CHS) with 4 column volumes for 5 times, then eluted using elution buffer (30 mM Tris-HCl pH 8.0, 150 mM KCl or 150 mM NaCl, 40 mM

maltose, 0.06% GDN or digitonin). The cells were further purified using SEC purification with FPLC Buffer (30 mM Tris-HCl pH 8.0, 150 mM KCl or 150 mM NaCl, 0.06% GDN or digitonin).

### **N-10x His tag-KCC3 Protein Purification**

Cells were resuspended in lysis buffer with Protease Inhibitor cocktail pills (Sigma-Aldrich). Then, cells were lysed using a Dounce homogenizer. Then, the detergent A (1% LMNG with 0.1% CHS or 1% DDM with 0.1% CHS) is added to the sample and stirred for 3.0 h at 4 °C to extract the membrane protein. The samples were ultracentrifuge at 40, 000 rpm for 1 hour to collect the supernatant containing membrane protein. The sample was incubated in cobalt beads and was collected in the Bio-Rad gravity column. They are washed using wash buffer (lysis buffer + 10 mM Imidazole) with detergent A with 4 column volumes for 5 times, then eluted using elution buffer (lysis buffer + 250 mM Imidazole + 0.06% GDN). The cells were further purified using SEC purification with FPLC Buffer

### **Nanodisc and Amphipol Reconstitution**

The lipid 1-palmitoyl-2-oleoyl-sn-glycerol-3-phosphocholine (POPC) solubilized in chloroform (Avanti) was dried and dissolved in 3% detergent buffer thoroughly at a concentration of 15 mM. KCC3 in the buffer after SEC was concentrated down to approximately 500 uL (Reid et al., 2020). To reconstitute KCC3 into nanodisc, the protein was mixed with MSP1E3D1 (Sigma-Aldrich) and lipid at a molar ratio of 1:3:140 (KCC3:MSP1E3D1: POPC) and was incubated at 4 °C for one hour (Reid et al., 2020). To reconstitute KCC3 into amphipols, the proteins are mixed

with A8-35 at a weight ratio of 1:4 (KCC3: amphipol) and were incubated at 4 °C for four hours. Bio-beads SM2 (Bio-Rad) are added four times within 24 h to remove the detergents from the system at a mass ratio of 20:1 (Bio-beads: detergents). Size-exclusion chromatography was used again to purify the reconstituted proteins from the empty Nanodisc.

### **Negative Stain EM Grid Preparation**

The purified protein from the SEC peaks were collected and diluted down to 0.02 – 0.03 mg/mL for negative stain EM grid preparation. The grids were prepared using negatively charged carbon coated grids supported by 400-mesh copper grids. 10 uL of the protein sample was loaded onto the carbon surface of the grid and was incubated for 1 minute. Then, the sample was blotted onto the filter paper. The grids were then washed with water droplet, blotted, washed again with water droplet, and then blotted. Finally, the grid was stained with 0.75% uranyl formate and blotted, which was also repeated twice. The grids were then dried via vacuum before being imaged using JEM 1400.

### **Cryo Electron Grid Preparation**

The proteins are collected from the SEC peaks and concentrated down to 1 – 10 mg/mL for the Cryo-EM study. 3uL of protein samples are added to the Quantifoil Holey Carbon grids (R1.2/1.3, Cu) and is blotted using Cp3 Plunge Freezer at >90% humidity for Cryo-EM data collection.

## **Result**

### **Protein expression and purification of N-MBP-PPX-KCC3b**

In an attempt to purify the KCC3 proteins to obtain the high-resolution protein structure, we started with N-MBP-PPX-KCC3b protein. Maltose-binding protein (MBP) was chosen as our affinity tag because it is one of the widely used tags that is shown to enhance the overexpression and the solubility of the membrane protein while maintaining its native function, making it suitable for structural and functional studies (Hu et al., 2011). Furthermore, Chew et al. (2019) and Yang et al. (2020) were able to successfully purify the protein and obtain the structure of cation chloride cotransporter using this tag. The tags were also added to the N-terminus of the protein because it was previously noted that the addition of any tags to the C-terminus may be detrimental to its function (Agez et al., 2017).

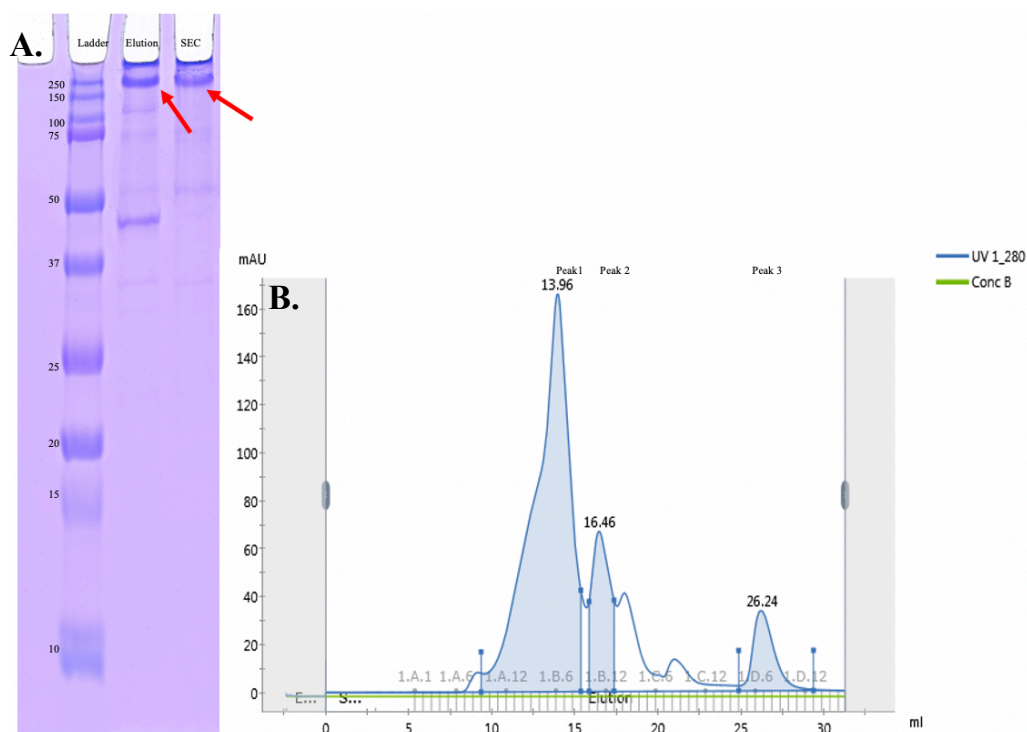


**Figure 1.** (A) SDS page gel of N-MBP-PPX-KCC3b protein after purification. The proteins are indicated with the red arrow. The expected size of our protein is ~240 kDa and is eluted using 40 mM maltose. Was further purified using Size Exclusion Chromatography (SEC). (B) SEC gel filtration profile of the N-MBP-PPX-KCC3b protein. Peak 1 is expected to be our protein, and was collected to run SDS page gel. Peak 3 is the maltose-binding protein.

Figure 1. illustrates the representative image (left) of the gel after the purification after eluting the samples with maltose using amylose beads and after Size Exclusion Chromatography (SEC), as well as the gel filtration SEC profile of the protein. The SEC sample in the SDS page gel corresponds to Peak 1 of the gel filtration profile. The expected size of our protein is ~240 kDa, which is clearly present in our gel (indicated with red arrow). The second band in our elution sample is probably the maltose-binding protein, which is isolated via gel filtration as peak 3. The SEC gel filtration was successfully able to isolate our protein sample into homogenous size, as indicated both in our SEC band in the SDS protein gel as well as our SEC profile.

### **Negative stain images of KCC3**

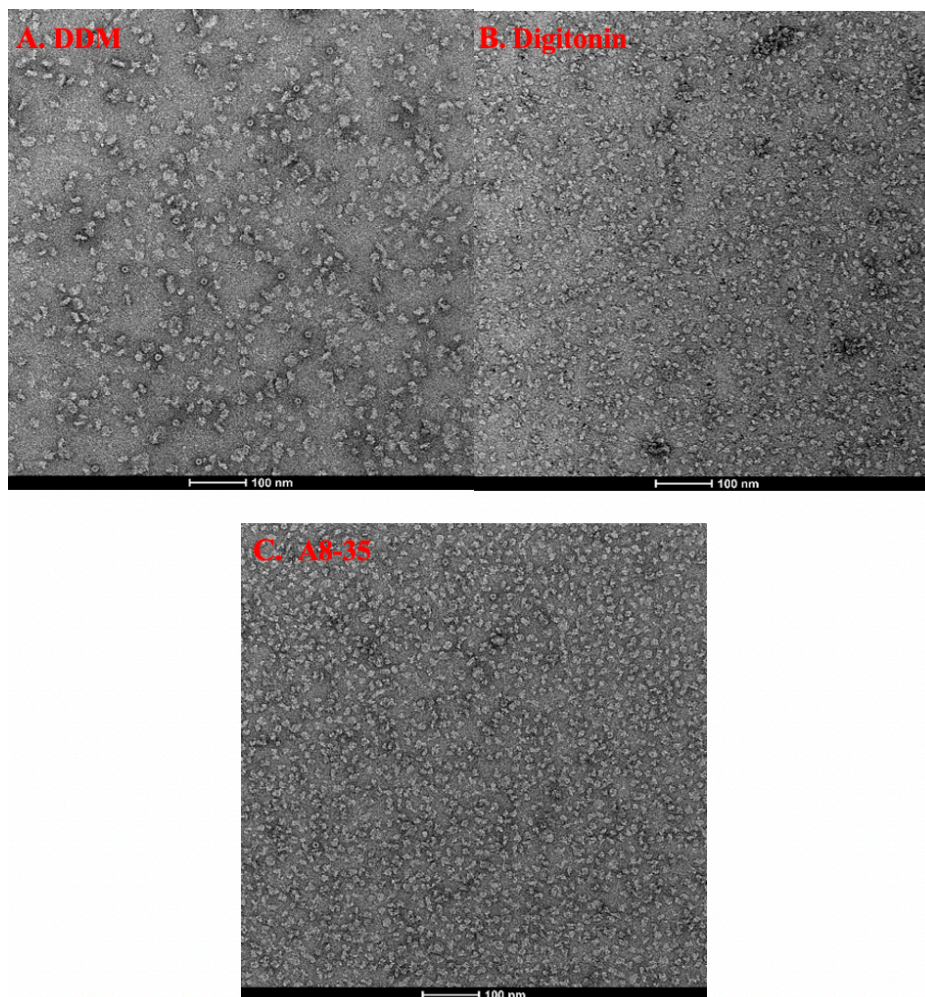


**Figure 2.** (A) Negative stain image of N-MBP-PPX-KCC3b protein after purification. (B) Negative stain image of N-MBP-PPX-KCC3b protein after reconstitution in Digitonin. (C) Negative stain image of N-MBP-PPX-KCC3b protein after reconstitution in A8-35.

As outlined in the method section, KCC3 proteins were first extracted using DDM/CHS and were reconstituted using various detergent agents and amphipols. After protein purification using amylose and SEC, the proteins were diluted to 0.05~0.06 mg/mL and negatively stained to visualize the general shape, size, and general homogeneity of the protein using an electron microscope. The label on the negative stain images above indicates the second detergents and amphipols that were used to reconstitute the protein after extraction.

As could be visualized on the images above, all proteins were relatively homogeneous with little aggregations. Proteins were also all very similar in size and shape, confirming that either of the detergents could be used to reconstitute the protein for our structural studies. Digitonin was chosen as our initial reconstitution detergent to prepare the grids for the cryo-EM studies because it is the most widely utilized detergent, having been used 30% of the published membrane protein structure (Choy et al., 2021), and because there has been a successful case study in which the high-resolution structure of the NKCC1 protein reconstituted in digitonin was obtained via Cryo-EM (Chew et al., 2019).

### **Cryo Grid Screening Images of KCC3**

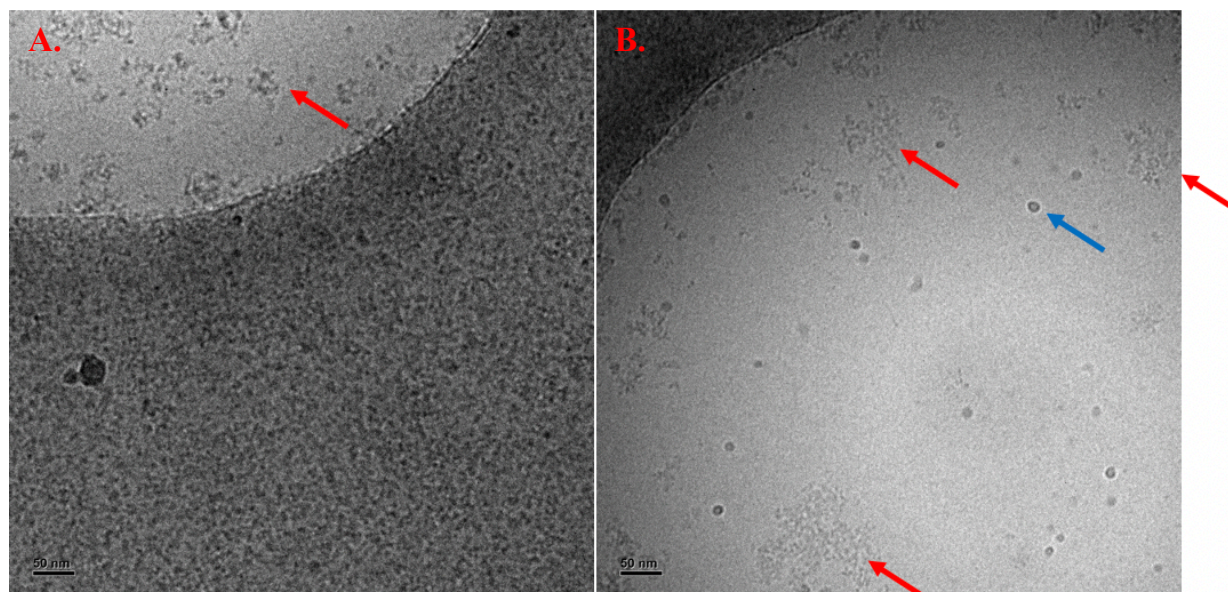


**Figure 3.** (A) Cryo grid image of N-MBP-PPX-KCC3b protein after reconstitution in digitonin. Many particle aggregation (red arrow) was observed in the screening image. Also, the particles seems to be all aggregated out of the carbon grid hole (light grey) into the copper support edge (dark grey). (B) Another view of the cryo grid image. The same particle aggregation (red arrow) was observed. Oil-drop-like particles (blue arrow) was also observed.

Above is a Quantifoil Holey Carbon Grid image of the KCC3-digitonin. Not only were many aggregations of the proteins observed (red arrow), but most of the particles seemed to be out of the carbon grid hole (light grey) onto the copper support edge (dark grey) which cannot be used for high-resolution structural elucidation. These problems can be attributed for several reasons: blotting time could be too long when our cryo grids were prepared using plunge-freeze that it made the vitreous ice layer too thin and pushed to proteins away from the center or that our sample may have had too little affinity toward the carbon grid (Supplemental Figure 5.) (Drulyte et al., 2018). Furthermore, many oil-droplets-looking particles were observed, which could be excess detergents (Liao et al., 2014). Overall, we hypothesized that detergent digitonin could cause protein aggregation, dissociate from the protein to form oil-droplet shaped micelles as well as also disturb

the surface tension of the water that would not make the digitonin a suitable candidate for the KCC3 cryo-EM studies (Liao et al., 2014; Autzen et al., 2019; Drulyte et al., 2018).

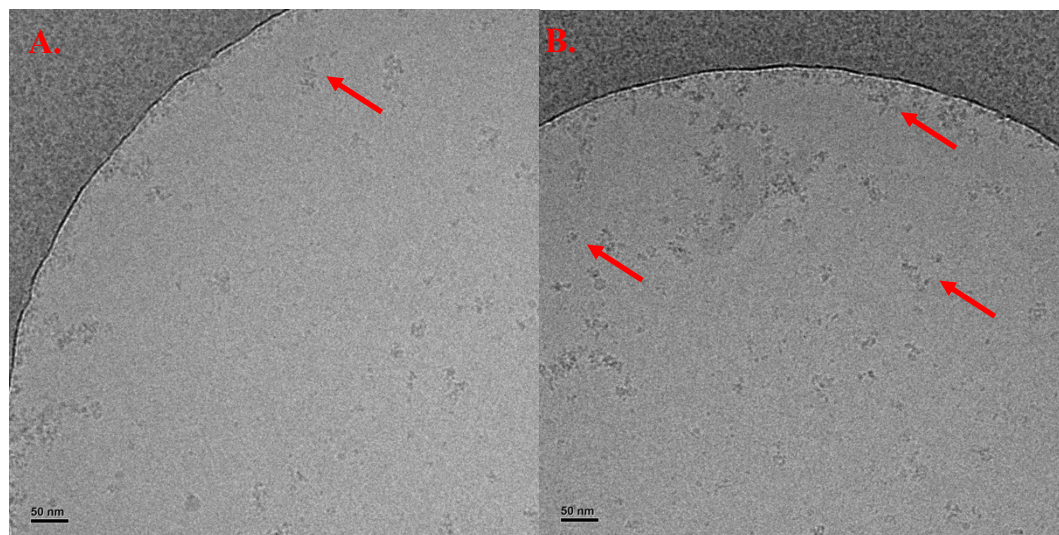


**Figure 4.** (A) Cryo grid image of N-MBP-PPX-KCC3b protein after reconstitution in amphipols. Many particle aggregation was observed in the screening image. Similar to the image observed in Fig 3. A, the particle also seems to have lower affinity towards the carbon grid hole (light grey). (B) Another view of the cryo grid image. The same particle aggregation (red arrow) was observed. No oil-drop-like particle was observed.

Above is a Quantifoil Holey Carbon Grid image of the KCC3-A8-35. A8-35 is a type of amphipol with a hydrophilic backbone that can substitute the detergent in the reconstitution process (Dorr et al., 2016). Compared to traditional detergents like digitonin, it has a higher affinity towards the hydrophobic transmembrane domain of the protein (Liao et al., 2014). Because it remains so tightly to the protein, it is less likely for it to dissociate from the protein to form aggregation by itself to create noise in the grid images.

Furthermore, any detergents that were used in the membrane protein solubilization process are removed from the protein sample, enabling it to bypass the negative influence that the

detergents may have on the cryo-grid samples (Sgro et al., 2018). Accordingly, no oil-droplet-looking particles, which were hypothesized to be formed from the excess digitonin, were observed in the cryo-grid images in the KCC3-A8-35 samples. Furthermore, there are fewer particle aggregations (Red arrow) observed in the KCC3-A8-35 samples than in the KCC3-digitonin samples.

However, protein aggregation is still observed in the grid. This could be possibly because the proteins were reconstituted in digitonin first before being replaced with A8-35 amphipols. The membrane protein tends to aggregate via hydrophobic regions of the TM region (Sgro et al., 2018), and the exposed transmembrane region in the KCC3-digitonin complex could have caused aggregation that was not reverted when it was attempted to be replaced by A8-35. Regardless, we still had the problem of the proteins aggregating mostly on the edge, some even being pushed (or attracted) out of the carbon grid hole towards the copper support.

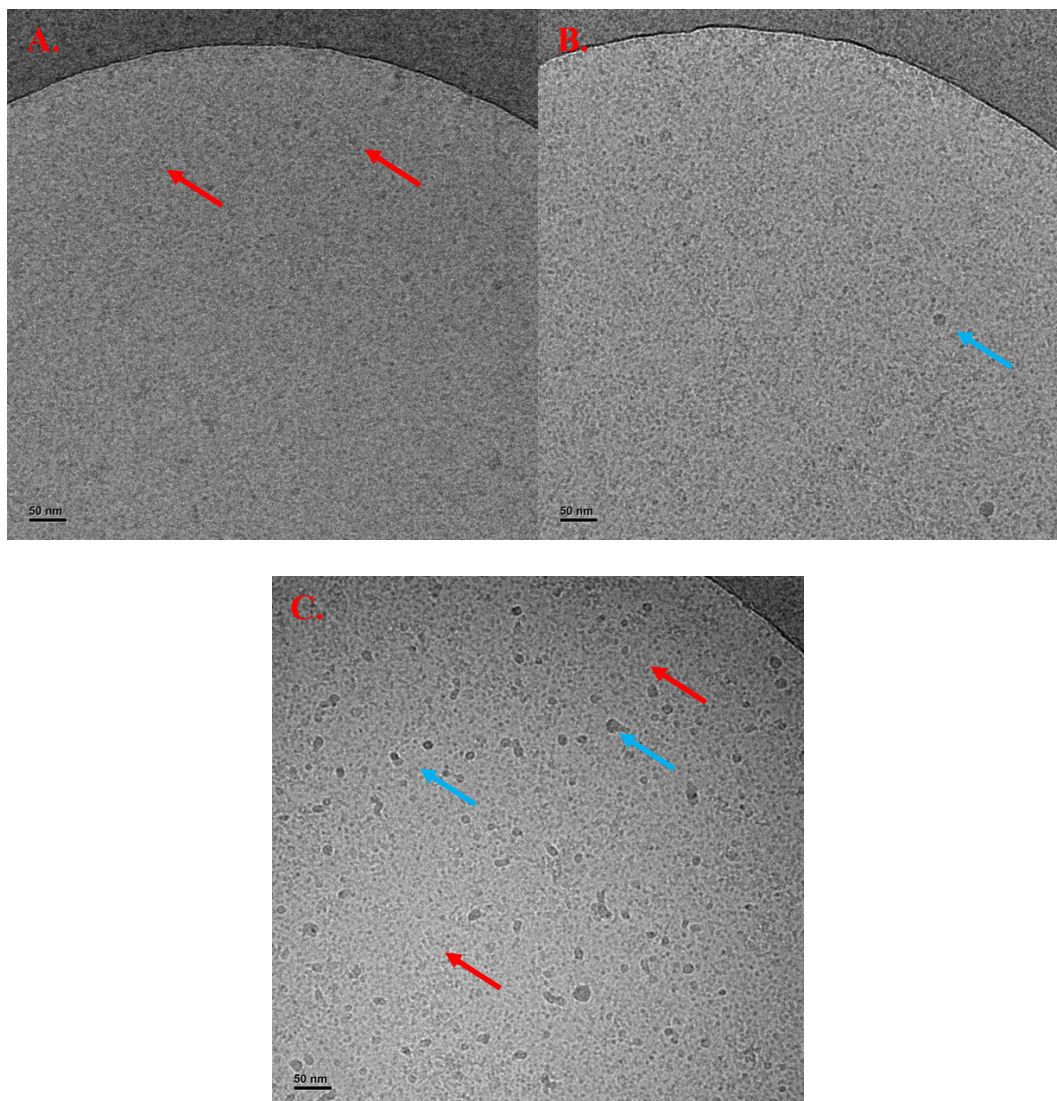


**Figure 5.** (A) Cryo grid image of N-MBP-PPX-KCC3b protein after reconstitution in GDN. Few, if any, particle aggregation was observed. The particle (red arrow) also seems to have relatively higher affinity towards carbon grid hole than previously observed in other detergent/polymer complex. (B), (C) Another view of the cryo grid image. GDN still being the detergent, the oil-drop-like particle was still observed (blue arrow).

Various other types of detergents were used to reconstitute the KCC3 protein and screened to identify the most optimal conditions for the cryo-grids. Most notably, we identified GDN to be the most optimal detergent that can be used to reconstitute the membrane protein for the cryo-EM

studies. GDN is a synthetic analog of digitonin that is becoming an increasingly popular detergent that is being used to exchange the detergent used in the solubilization process (Choy et al., 2021). It has relatively low-critical micelle concentration (CMC), more soluble in water, and less batch-to-batch variability than digitonin (Sgro et al., 2018). Furthermore, the recent study has shown success in obtaining the structure of the KCC1 protein reconstituted in GDN via cryo-EM (Liu et al., 2019).

Most notably, fewer protein aggregations in the KCC3-GDN sample (red arrow) are noted in the cryo-grids, and KCC3-GDN seems to have a higher affinity towards the carbon grid hole than the KCC3-A8-35 and KCC3-digitonin samples. Furthermore, fewer micelles were observed in the KCC3-GDN cryo-grid samples than the images in KCC3-digitonin samples, which could be attributed to its lower CMC (Choy et al., 2021). However, given that GDN is still a detergent, the micelle formation was not completely avoidable in the KCC3-GDN complex as the oil-droplet-like particles (blue arrow) were still observed in some carbon grid holes.

Regardless, enough particles were able to be picked in the KCC3-GDN sample to advance to cryo-EM image processing.

## Cryogenic Electron Microscopy Image Processing

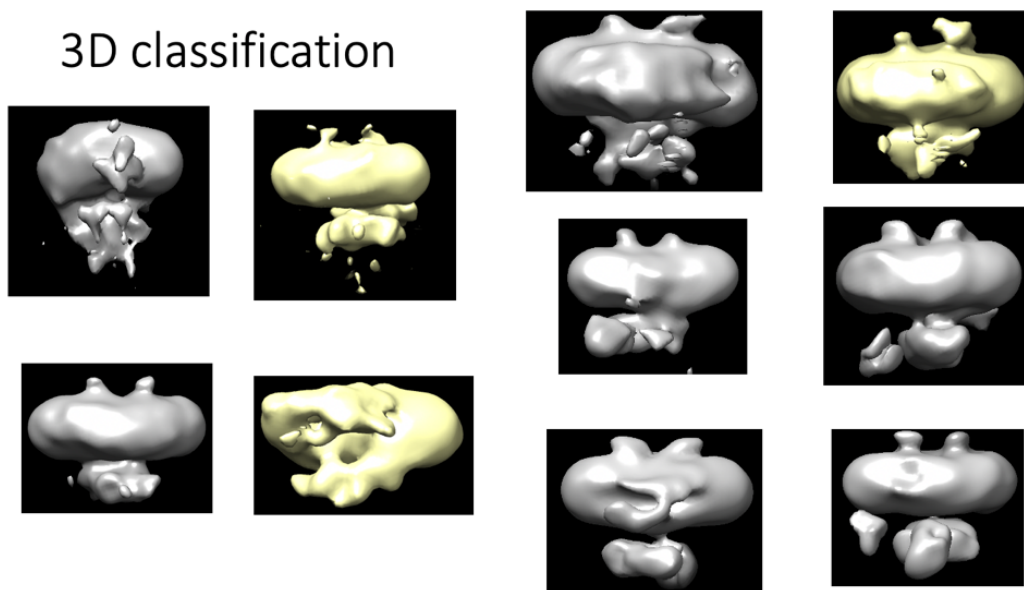


**Figure 5.** Images obtained from the different 3D classification images using the KCC-GDN particles obtained from the cryo-EM images.

First, the single particles were selected using the RELION program to be processed for a higher resolution structure (Supplemental Figure 6.). After the selection, different 2-D classifications of the particles were obtained to identify the obviously bad unwanted images, as well as to sort heterogeneous structures (Supplemental Figure 7.). Lastly, 3D classification is applied to sort the particles into distinct homogenous populations, in which the different 3D reconstructions can be compared and superimposed to reconstruct the single particles.

The above images represent the different 3D classifications obtained from the KCC3-GDN cryo-grids. Unfortunately, the structure could not be pushed to a higher resolution than 9Å, which prevented the scrutinization of the protein to molecular details. The 2D and 3D classifications, however, were very similar to the recently published NKCC1 and KCC1 protein, confirming that

the 3D reconstructions obtained are the KCC3 proteins in dimer formation (Liu et al., 2019; Chew et al., 2019) unlike the KCC4 structure which were obtained in the monomer structure (Reid et al., 2020). Our relatively lower resolution could have been due to a relatively big MBP tag (43 kDa) that was connected to the KCC3 protein via a flexible linker sequence that negatively impacted the image alignment of the protein in the 3D reconstruction process of the modeling. In fact, the MBP tag was cleaved from the NKCC1 protein before its high-resolution structure was obtained via cryo-EM (Chew et al., 2019). Unfortunately, however, the MBP tag could not be cleaved from our protein because reducing agents were required for the precision protease activity; reducing agent could not be used in our protein as it was indicated in the KCC1 structure that the big extracellular between TM5 and 6 were rigidly stabilized by the extracellular disulfide bond and reducing agent may denature KCC3 protein (Liu et al., 2019).

As a result, a new gene construct was synthesized with a smaller affinity tag (N-10x his tag-KCC3).

## Transformation and Plasmid purification of N-10x His tag-KCC3

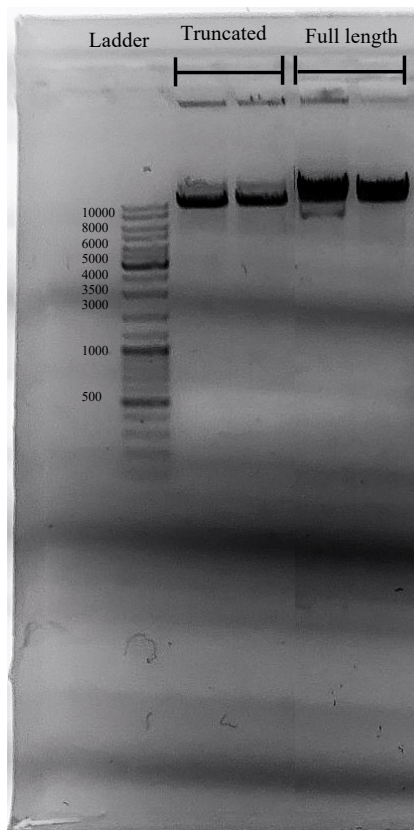


**Figure 6.** Gel electrophoresis image of the N-10x his tag-KCC gene plasmid after plasmid purification and linearized using DpnIII digestion. Truncated gene expresses N-truncated KCC (109-1099). The single band indicates the purity of our plasmid.

Above is the gel electrophoresis image of the linearized plasmid after the purification using Gigaprep kit (Qiagen) transformation of the newly synthesized KCC3 plasmid. The truncated refers to the gene construct in which the gene responsible for the expression of the N-terminus of the KCC3 (1-109) has been truncated. The single band, as well as the relative positions of two gene construct, confirms that we were able to successfully transform, amplify, and purify our plasmid of interest. It should be noted that the yield of the full-length plasmid

tends to be lower than the truncated (Supplemental Fig 9.) which could indicate that the full-length plasmid may be toxic or was not well transformed into the *E. coli* cells that were used to amplify the gene.

### **PEI-based Transfection**

As described in the introduction section, Polyethylenimine (PEI) based transfection involves PEI condensing the plasmid DNA into the positively charged particles so that it binds to the anionic cell surface of the mammalian cells and is introduced into the cells via endocytosis (Longo et al., 2013). There are mainly two methods to transfect the plasmid DNA using PEI: 1) Adding DNA first into the cell culture followed by adding PEI (Subedi et al., 2015); and 2) Incubate to form DNA and PEI first to form DNA/PEI complex first before introducing them into the cells (Portolano et al., 2014).

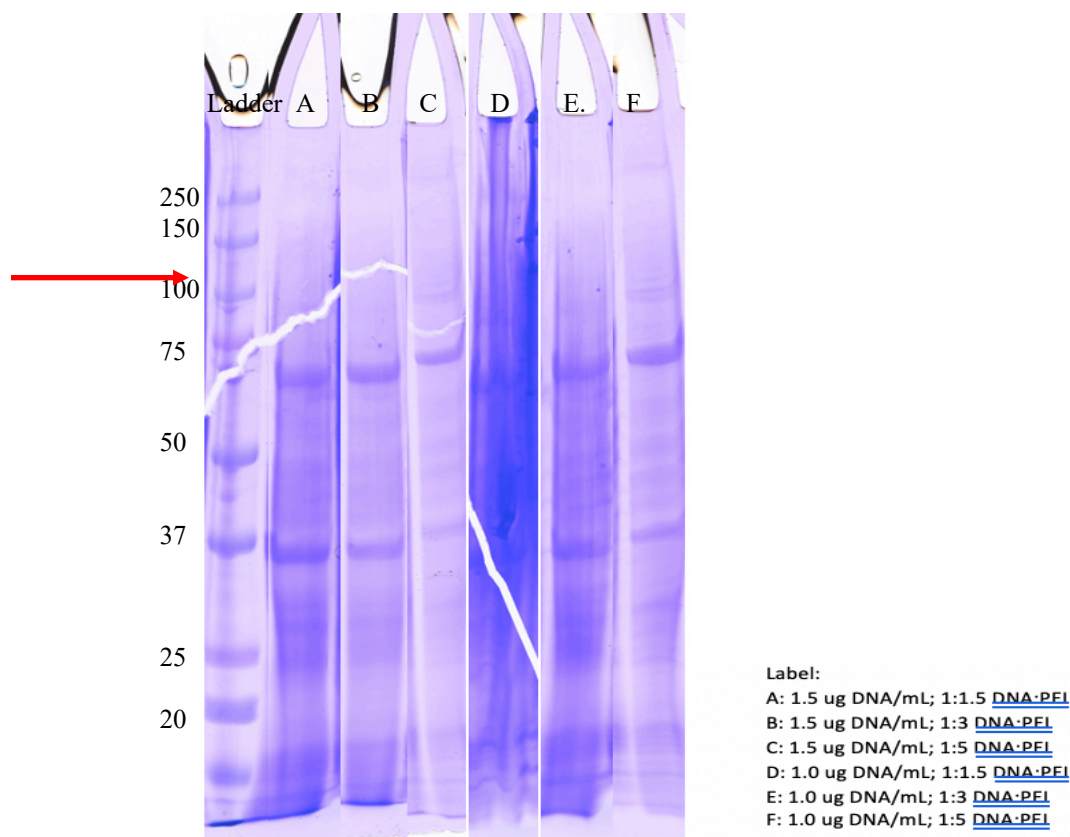


**Figure 7.** SDS page gel of the protein after protein purification after the protein was expressed using the PEI-based transfection method 1 with varying DNA: PEI ratio and DNA concentration. The N-10x his tag-KCC is expected to have a size ~113 kDa. No bands were observed in an area that corresponded to the size of our protein, meaning method 1 may not be the most ideal method

Figure 7. is the SDS page gel of the protein after purification using method 1 in which DNA and PEI were introduced to the cell culture separately with varying DNA: PEI ratio and DNA concentration. As indicated in the gel above, no bands were observed in around 113 kDa where we expect our protein to be (red arrow). No bands were also observed in our small volume expression test in which the whole cells were lysed 24, 48, 72, and 98 hours after the transfection (Supplemental figure 9). This could be partly because DNA and PEI were too diluted in the cell

culture that they were seldom able to interact with each other for PEI/DNA complex to form for endocytosis.

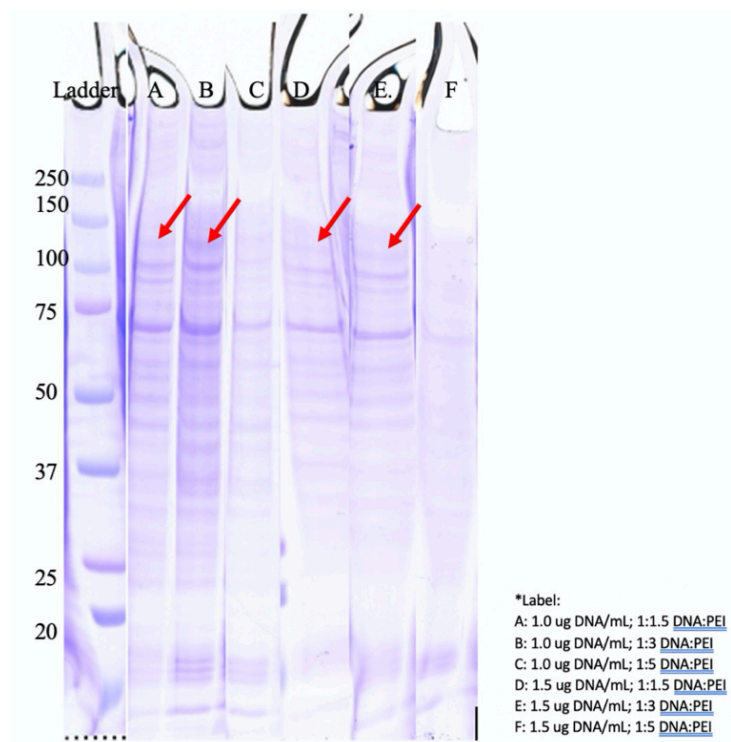


**Figure 8.** SDS page gel of the protein after protein purification after the protein was expressed using the PEI-based transfection method 2 with varying DNA: PEI ratio and DNA concentration. The N-10x his tag-KCC is expected to have a size ~113 kDa. The clear bands (red arrow) were observed at around ~113 kDa. Notably, no bands were observed at either of the DNA concentration when they were transfected with DNA:PEI ratio of 1:5. The clearest band was observed at the DNA: PEI ratio of 1:3.

Figure 8. is the SDS page gel of the protein after purification using method 2 in which DNA and PEI were introduced to the cell culture separately with varying DNA: PEI ratio and DNA concentration. Compared to the SDS page gel with method 1, a clearer band was observed at 113 kDa (red arrow). It is important to note that no proteins were expressed when the DNA: PEI

complex was formed at the ratio of 1:5, hinting that too much PEI can negatively influence either the protein expression or transfection. All bands were poorly enriched, indicating that the protein expressions are overall low. The bands were most enriched when the DNA: PEI complex was formed at the ratio of 1:3 (B), so further attempts were done to find the most optimal conditions for protein expression.

It must be noted that the PEI and DNA should be diluted to 0.3 ug/mL each with the cell media before they are combined to form the complex. When they were combined without such dilution, the PEI/DNA complex precipitated out of the solution, which could have negatively impacted the transfection efficiency. In fact, some studies use concentrated PEI to precipitate the nucleic acid impurities from the target protein during the purification process (Burgess, 1991).

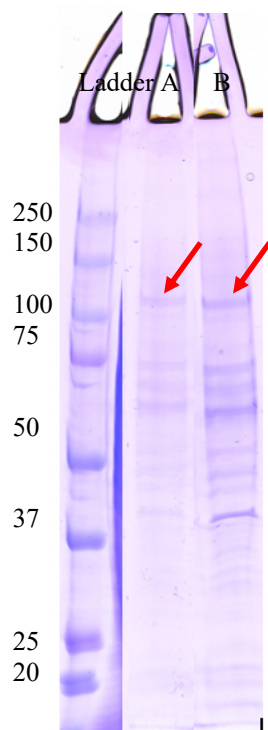


**Figure 9.** SDS page gel of the protein after protein purification after the protein was expressed using the PEI-based transfection method 2 at 1:3 DNA:PEI ratio. To increase the transfection efficiency, the cells were supplemented with valproic acid 3 hours post transfection (A) or with sodium butyrate 24 hours post transfection (B) at 37 °C.

To increase the transfection efficiency as well as protein expression level, the cells transfected at different conditions with different supplements and temperature (Supplemental Figure 10.). It was determined that the cell transfection with DNA with PEI at the ratio of 1:3 (DNA:PEI) with either 3mM valproic acid (A) or 20 mM sodium butyrate (B) supplement at 30°C has increased the most transfection efficiency. It was also previously noted that lowering the incubating temperature from commonly culturing temperature of 37°C slows down the cell growth and increased the protein expression by 1.5 fold in HEK293 cells (Lin et al., 2015; Schlaeger and Lundstrom, 1998). Valproic acid is also shown to increase the transfection efficiency (Cervera et al., 2015). Valproic acid is a short fatty acid chain that causes hyperacetylation of histone H3 and

H4 (Marchion et al., 2005). It is previously shown that valproic acid enhances the recombinant gene expression (Fan et al., 2005). Sodium butyrates are histone deacetylase inhibitor that inhibits the proliferation of HEK293 (Li et al., 2015), which are shown to increase recombinant protein expression (Ansorge et al., 2009).

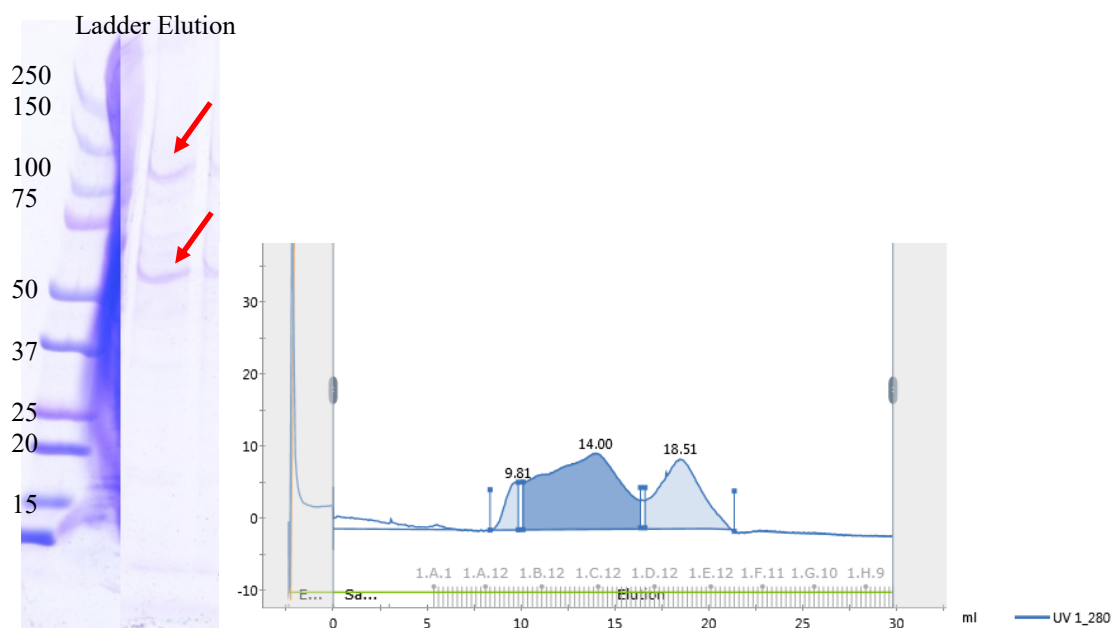


**Figure 10.** (A) SDS protein gel after protein purification of larger HEK293 cell volume (800 mL) using Cobalt beads. As expected, the clear bands were observed at around 113 kDa. (B) SEC Gel filtration profile of the KCC3 protein. Our protein expression is not yet high enough to proceed to electron microscopy studies. As a result, further optimization must be done to increase the transfection efficiency.

At last, now that the most optimal conditions for protein expression were decided, we began a larger volume of transfection. Above is the protein purification gel of 800 mL of HEK293 cells that were transfected with DNA and PEI at the ratio of 1:3 (DNA: PEI) at 30 °C supplemented with valproic acid. Valproic acid was chosen because it is more widely used for transient PEI-

based transfection and lower toxicity (Subedi et al., 2015; Fan et al., 2005). As expected, we see a much clearer band at around 112.9 kDa (Red arrow), where we expect to see our protein.

The right gel filtration profile shows, however, that our protein expression is not yet high enough to proceed to electron microscopy studies. As a result, further optimization must be done – perhaps higher cell volume transfection.

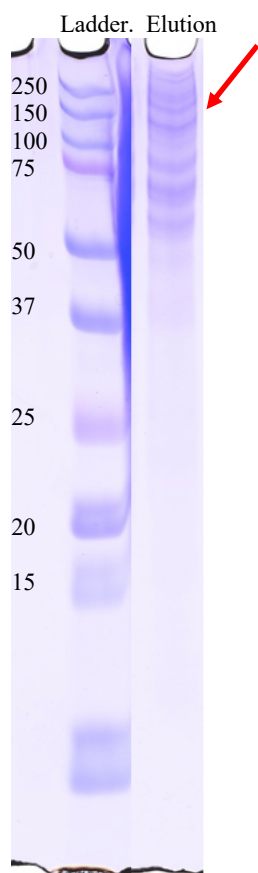


**Figure 11.** SDS page gel of the protein after protein purification using nickel beads after protein expression at 1:3 DNA:PEI ratio supplemented with 3 mM valproic acid. While the bands of our protein (red arrow) are clearer, proteins seems to bind relatively at lower specificity to the Ni beads than Cobalt beads. Further optimization must be done to isolate our protein.

Purification of the protein using nickel beads were attempted to increase the yield of our protein. Nickel beads tend to have a higher affinity for his-tag, so the 800 mL cells were transfected

using the same method used before. Above represents the gel that was eluted with gradient imidazole concentration. While the bands were more enriched indicating a higher yield of our protein, they are also less pure, indicating that the nickel beads are not too specific enough and not be able to be used to obtain the homogenous, pure samples to proceed to electron microscopy studies. Further optimization must be done before the study can take the protein samples to microscopical studies.

## Two Additional Studies Using Similar Techniques

### Gel Filtration Profile and Negative Stain EM to Characterize the Protein (Gao et al., 2019)

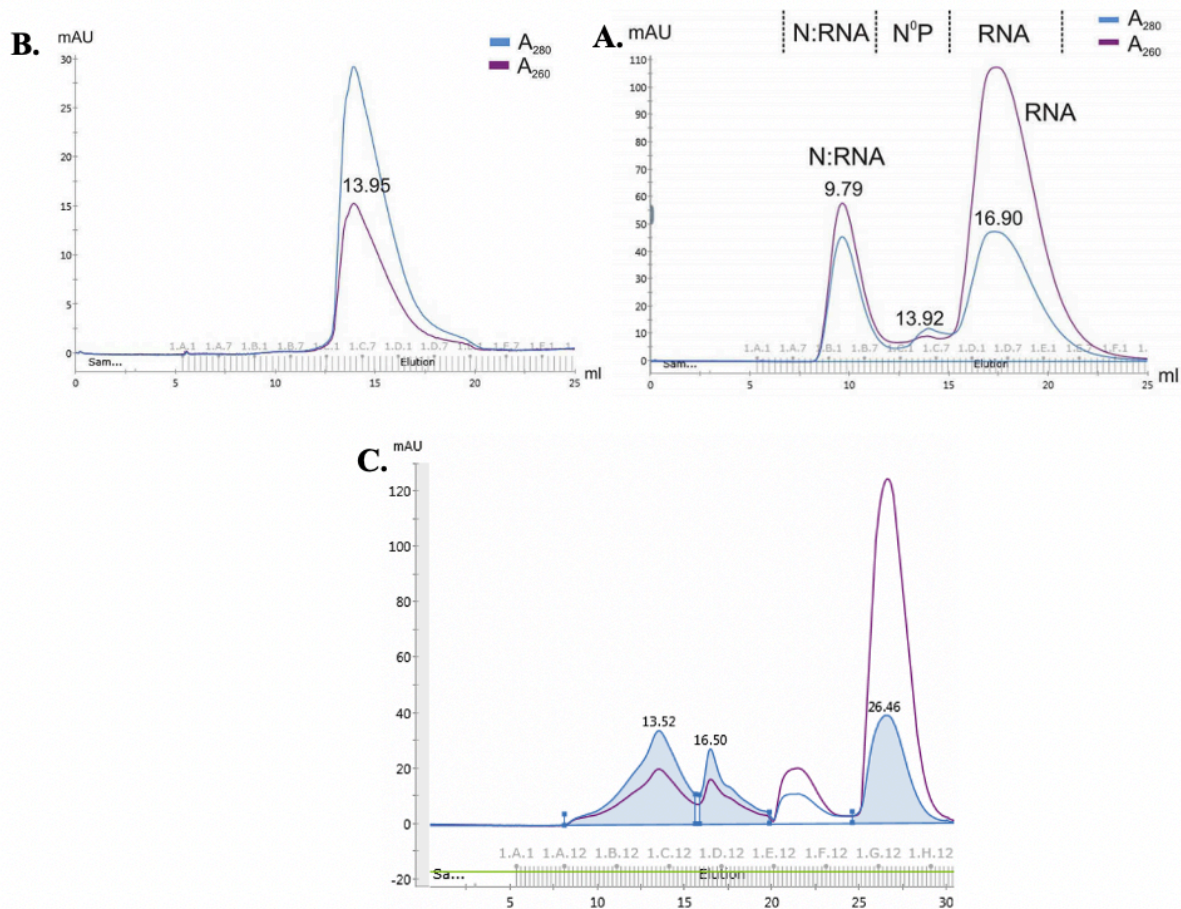


**Figure 12.** (A). Representative gel filtration profile of  $N^0P$ .  $A_{280}/260$  ratio is  $\sim 0.6$ , indicating that they are pure protein complex without any nucleic acid impurities. (B) Representative gel filtration profile characterizing N-RNA complex assembly. The first peak corresponds to N-RNA complex. The second peak corresponds to the  $N^0P$  complex. The third peak corresponds to the RNA that is not associated with the N protein. (C) Representative gel filtration profile characterizing KCC3 protein. The  $A_{280}/260$  ratio of peak 1 indicates that our KCC3 protein is a protein without any nucleic acid impurities.

To confirm the purity of the protein samples, the SEC gel filtration profile was used to examine the A260/280 ratio of each peak. Ideally, the pure protein without any nucleic acid must be at around 0.6. For example, the above graph (A and B) represents the gel filtration profile of our previously published article which used negative stain EM and gel filtration profile to characterize the *in vitro* assembly of RSV nucleocapsid (N) protein of the RNA (Gao et al., 2019). In this study, N proteins were co-expressed with the N-terminus of the RSV phosphoprotein (P) to form N<sup>0</sup>P complex and regulate the N protein from binding nonspecifically to the RNA (Gao et al., 2019). We have shown in this study that RSV-specific RNA can be added to stimulate and replace the P protein from the N<sup>0</sup>P complex to form the N-RNA complex.

Graph A, as could be seen from its A280/260 ratio, shows the pure N<sup>0</sup>P protein without any nucleic acid (i.e. RNA) impurities. On the contrary, graph B shows three different peaks with varying A280/A260 ratios: 1) N: RNA peak with  $0.6 < n < 2.0$  A280/260 ratio which indicates protein-RNA complex; 2) N<sup>0</sup>P peak with  $\sim 0.6$  A280/260 ratio which indicates pure protein complex; and 3) RNA peak with  $\sim 2.0$  A280/260 ratio which indicates pure RNA samples. Since our current study only involves pure KCC3 protein without nucleic acid, the A280/260 ratio should ideally be  $\sim 0.6$ . Graph C represents the gel filtration profile of the protein after being reconstituted in detergent digitonin. As could be seen in the A280/260 ratio of peak 1, we have confirmed that our protein was not contaminated by any nucleic acids.

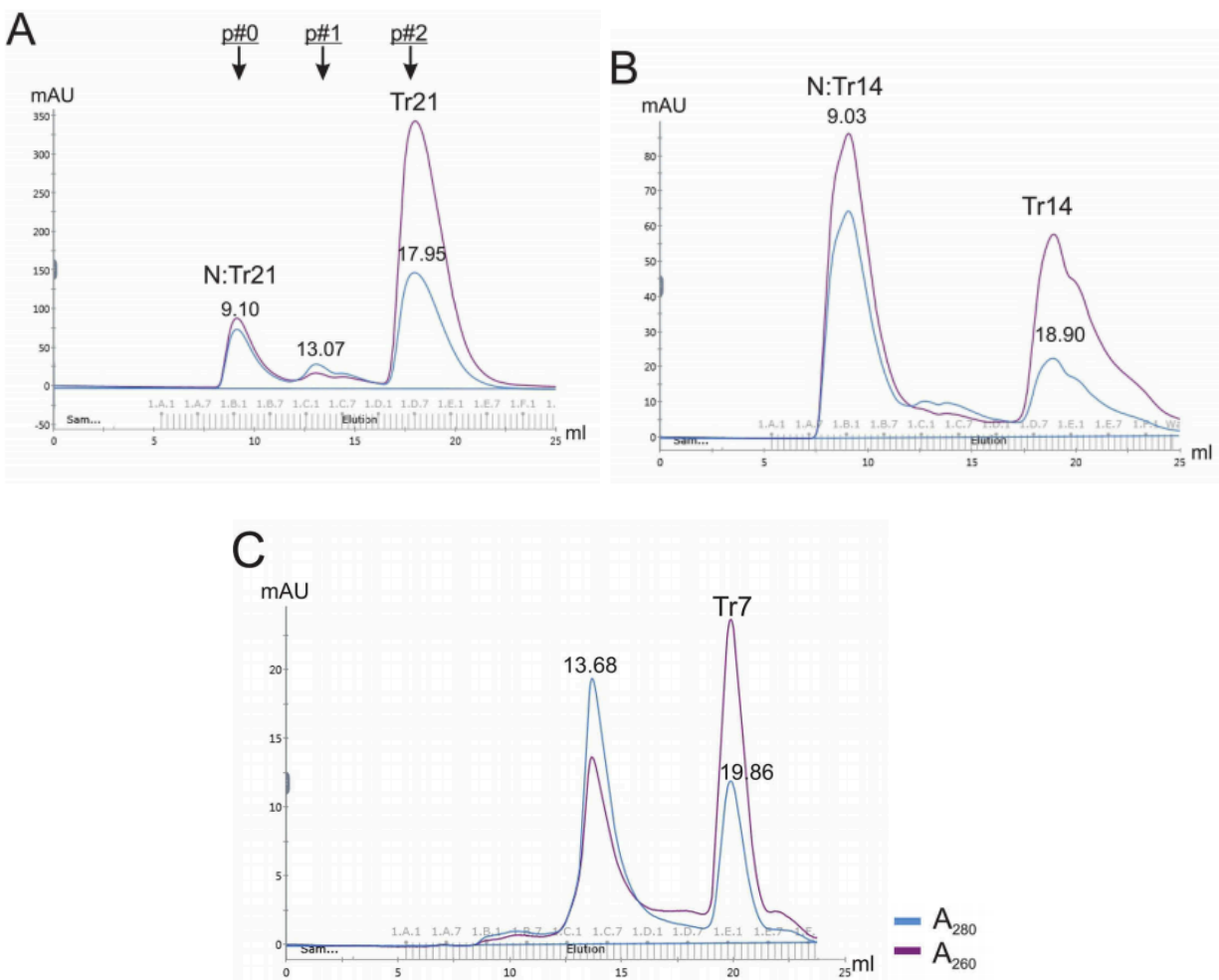


**Figure 13.** Representative gel filtration profile characterizing the N-RNA assembly with RNA of varying length – 21 nt (A), 14 nt (B), and 7 nt (C). The  $A_{280}/A_{260}$  ratio indicates that the N-RNA only occur with 21 nt and 14 nt RNA (A), (B). The ratio also suggests that the N-RNA complex assembly may not occur at the factor of 7 nt as was previously suggested.

Similarly, multiple gel filtration profile was obtained to characterize the length preference for N-RNA complex assembly. The  $N^0P$  complex was incubated with 21 nt, 14nt, and 7nt of the RSV genomic trailer sequence and was examined using the SEC gel filtration graph. As could be seen from the graphs above,  $N^0P$  formed N-RNA complex only with 21 nt (graph A) and 14 nt (graph B) RNA, but not with the 7 nt RNA (graph C). This is quite surprising, given that it was

previously suggested that N protein binds to every 7 nt RNA (Cowton et al., 2006). It was hypothesized that this could be because the N-protein may not bind to the first nucleotide of the RNA. In fact, it should be noted that A260/280 of the N-RNA complex with 14 nt is higher than the A260/280 of the N-RNA complex with 21 nt. If N protein all interacted with RNA at position 1 of the RNA, they would be tightly packed and the A260/280 must have a similar value; However, such observation was not observed in the above graph. In fact, the graph above seems to indicate that the RNA:protein ratio of the N-Tr14 complex seems to be higher than the RNA:protein ratio of the N-Tr21 complex.

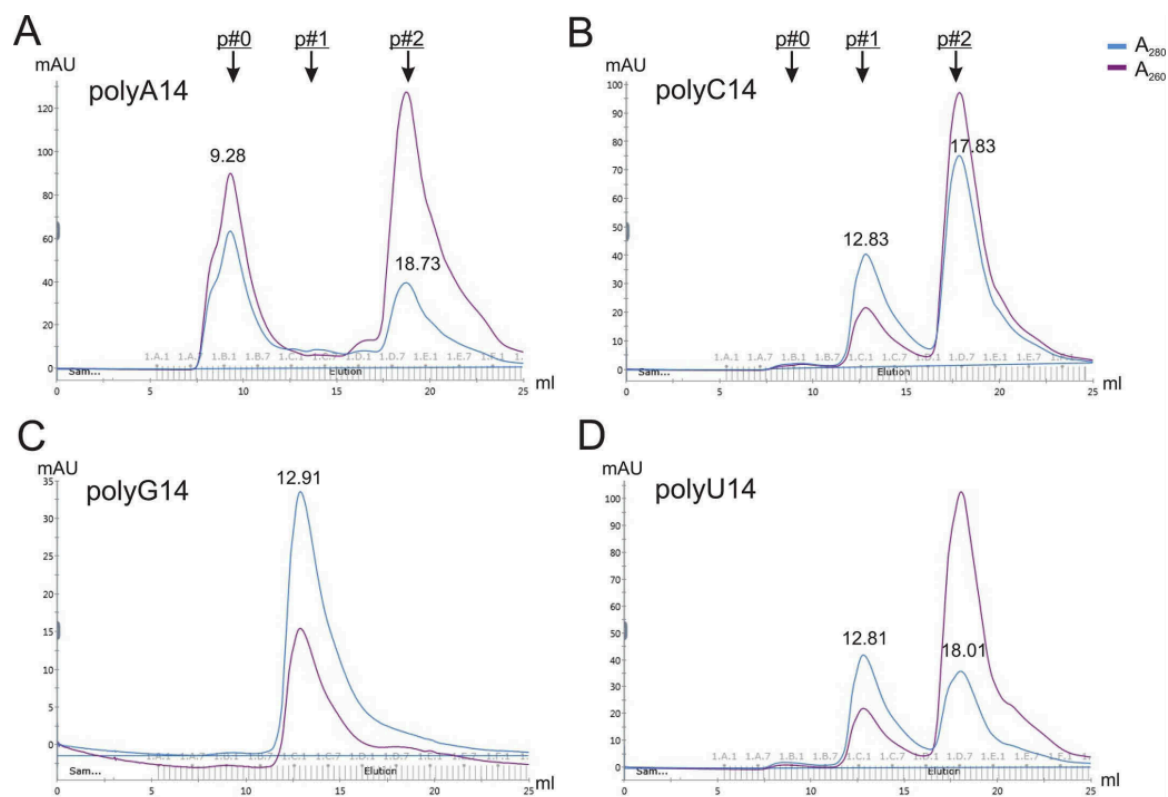


**Figure 14.** (A)-(D) Representative gel filtration profile examining the preference of specific RNA nucleotide for N-RNA assembly using 14 nt RNA. N-RNA assembly only occur with polyA RNA (A), indicating that N<sup>0</sup>P has a clear preference towards A nucleotide.

Furthermore, gel filtration profile was used to examine the preference of specific RNA nucleotide that the N protein may prefer using the 14 nt RNA. As evident from the profile above, the N protein has a clear preference for adenosine nucleotide.

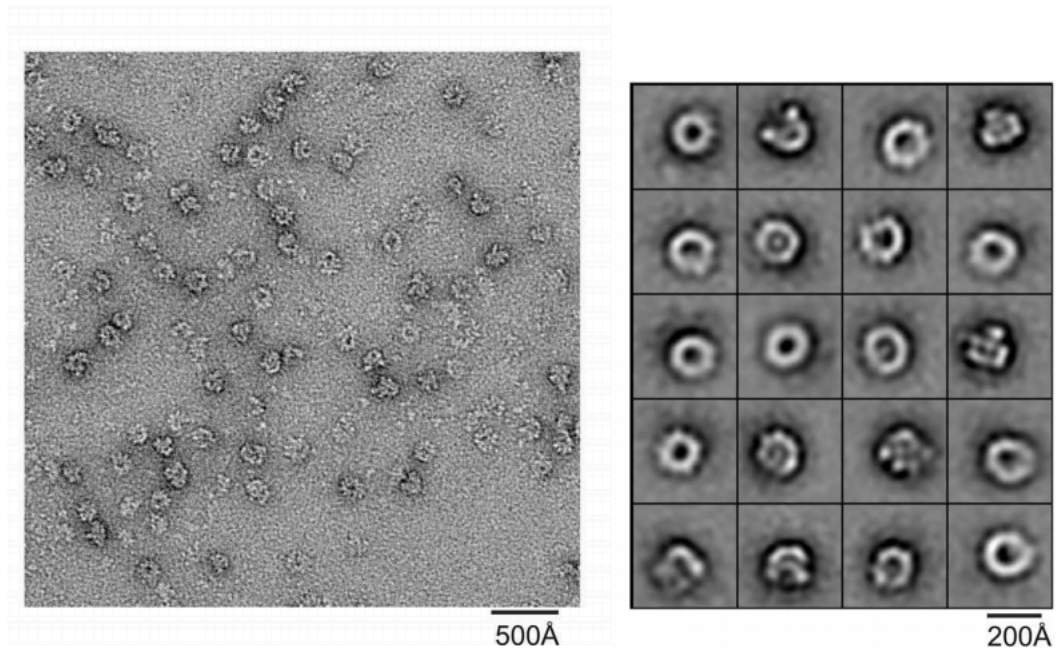


**Figure 15.** Representative negative stain EM image of the N-RNA complex.

Lastly, negative stain images of the N-RNA complex were obtained to characterize the general shape of the particle. They indicate that the N-RNA complex resembles a ring-shape structure.

## High Resolution Structure Involving His-tag Purification and Protease Cleavage

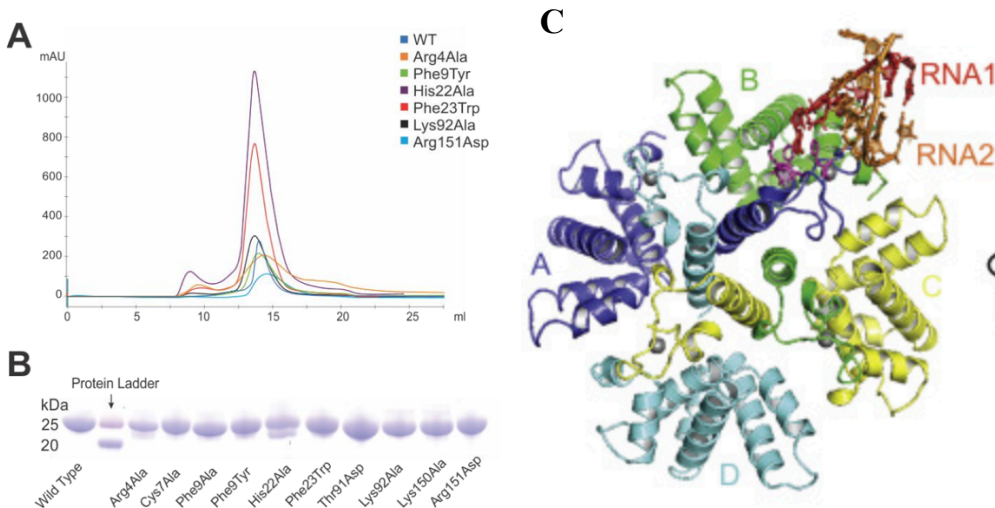


**Figure 16.** (A) Representative SEC gel filtration profile of WT and mutant M2-1 protein after his-tag purification. (B) Representative SDS page gel of WT and mutant M2-1 protein. (C) The general crystal structure of M2-1 interacting with the 7 nt RNA. Note that the complex was crystallized with the four M2-1 protomer.

In our previous study, we have determined the crystal structure of the HRSV M2-1 in complex with 7-nucleotide positive-sense gene end RNA at 2.7 Å (Gao et al., 2020). The complex was crystallized with 4 M2-1 protomers. M2-1 is a transcriptional anti-terminator, one of the four essential proteins (other being phosphoprotein P, nucleocapsid protein N, RNA-dependent RNA polymerase L) required for transcription (Collins et al., 1996). They are hypothesized to bind to the growing RNA strand, preventing premature termination via stabilizing interaction with the transcription complex. Overall, it is indicated in this study that his-tag purification can be used to purify the protein for the structural study purposes. Because the target protein (M2-1) of this study is an intracellular protein, protease cleavage could be applied with 1mM DTT while preserving the native structure of the protein.

## **Discussion**

### **PEI-based transfection of N-10x his tag-KCC3**

In this study, we have optimized the protocol for PEI-based transient transfection for the suspension HEK293F cell culture. While there have been few established protocols for the PEI-based transient transfection for the suspension cell culture (Subedi et al., 2015; Portolano et al., 2014), most of the PEI-based transient transfections were done for the cell culture at smaller volume (Longo et al., 2013). Because structural studies often require proteins in the order of milligram for X-ray crystallography and in the order of microgram for cryo-EM (Liao et al., 2014), being able to transfect the cells at higher volume for recombinant protein expression is very important to obtain the high-resolution 3-D structures. PEI-based transfection to introduce the DNA to the cell is more beneficial than the viral method due to its lower cost, toxicity, immunogenicity, and less time-consuming (Aslan et al., 2006). We further demonstrated that we can use supplements such as histone acetylase (VPA) and histone deacetylase inhibitors (sodium butyrate), as well as lower temperatures for a higher yield of our recombinant proteins.

### **N-terminus purification tag**

In both of our gene constructs, we added a protein purification tag to the N-terminus of the KCC3 protein. It was previously shown in the KCC2 that the addition of any protein purification tag completely abolished the transporter activity without affecting the protein's expression level and membrane localizations (Agez et al., 2017). Furthermore, when we hypothesized that the relatively big purification tag MBP could play a key role in our inability to push the structure of the KCC3 protein to the higher resolution, we refrained from cleaving the tag using Precision Protease because it required reducing agents such as DTT (Ullah et al., 2016). The previously

published cryo-EM KCC1 structure shows that the big rigid extracellular loop is stabilized by the disulfide bond (Liu et al., 2019), and it was shown in the KCC2 architecture studies that DTT significantly reduced the dimerization of the KCC2 protein (Agez et al., 2017). Lastly, it was suggested that abolishing this disulfide bond downregulates the activity of the transporter (Joiner et al., 2004). Furthermore, NKCC1 cryo-EM structures suggest that N-terminus may not play a substantial role in structural determinations, given the structural similarity between the full length and truncated NKCC1 (Chew et al., 2019). As a result, some of our recombinant proteins were designed with truncated N-terminus.

### **General Architecture and Electron Microscope Images of N-MBP-PPX-KCC3b**

We demonstrate the overall architecture and the general shape of the KCC3 structure using the 2D classification images and the 3D reconstruction images. While we were not yet able to obtain the structure with good enough resolution to scrutinize the structure to atomic details, the 2D classification images and 3D reconstruction images suggest that KCC3 protein may form a dimer structure. Furthermore, the 3D modeling of the KCC3 was comparable to the dimeric KCC1 proteins obtained by Liu et al. (2019), unlike the monomeric KCC4 structures obtained by Reid et al. (2020), further validating our conclusion that KCC3 obtained in our study was in dimeric form.

Next, we also characterized the electron microscopy images of the KCC3 protein in different detergents and polymers. While our negative stain images were able to yield relatively homogeneous particles for all protein-detergent complex, cryo-grid yielded variable results depending on the different detergents used for reconstitution. For example, we demonstrated that using a detergent with high CMC, such as digitonin, may negatively influence the quality of the

cryo-grid images by disturbing the surface tension of the water, causing protein aggregations, and dissociating from the proteins to form micelles (Sgro and Costa, 2018). Furthermore, we illustrated that while the KCC3-amphipol complex was able to eliminate the disturbances from the micelle formations that the digitonin detergent has introduced, the KCC3-amphipol complex still had the problems of protein aggregations and being pushed out from the center of the hole. While the reason for KCC3 proteins having a lower affinity towards the carbon grid hole is unknown, we hypothesize that the KCC3-amphipol complex was still aggregated because amphipol reconstitution still requires the protein to be solubilized in digitonin detergent first. We suspect that the protein aggregation was formed in the KCC3-digitonin phase, and the amphipol's affinity towards the hydrophobic transmembrane region of the protein could not have been high enough to overcome the hydrophobic interactions between the proteins even with the amphipol's high affinity towards the protein's transmembrane region (Liao et al., 2014). Lastly, we determined that the KCC3-GDN complex formed the most ideal sample grids for the cryo-EM studies, with even distributions in the vitreous ice layer without much aggregations (Drulyte et al., 2018).

## **Known Structural Insights into KCC Families**

### **Structural Analysis of KCC1**

Liu et al. (2019) have been able to find the first 3-D high-resolution structure of the KCC1 through Cryo-EM. They were able to solubilize the protein in three different conditions: in 150 mM KCl with GDN, 150 mM NaCl with GDN, and 150 mM KCl with nanodisc (fig 9). The membrane scaffold protein used for nanodisc formation was MSP1E3D1 with lipid POPC. Here, they were able to identify that KCC1 has 12 transmembrane helices with both amino and carboxyl terminus in the intracellular cytoplasm<sup>8</sup>. The TMD region adopts the LeuT-like fold.

The dimerization is stabilized by the TMD and extracellular loop of the protein. Because KCC1 structure in this study had relatively lower resolution in the CTD, the domain was excluded in the structural study, preventing any analysis on its possible role in dimerization and function. Regardless, many previous studies have indicated that KCC1 dimerization may still occur in the absence of the C-terminal domain (Casula et al., 2009; Simard et al., 2007; Uvarov et al., 2007). The transmembrane domain that is involved in the dimer interaction involves TM12 and TM9 which the hydrophobic residues of TM12 interact with the adjacent residues in the TM9 and also the interior hydrophobic cavity between the monomer. In the extracellular loop interaction, it is noted that the hydrogen bond between the carboxyl oxygen of S403 and the amine group of K405 is important as well as also the hydrophobic interactions in the P355, P402, and L404. It seems like the extracellular loop may play a more important role than the TMD in the interaction as single or multiple mutations in the TMD dimer interface did not significantly disrupt the dimerization (Liu et al., 2019). While the direct relationship between the disulfide bond and dimerization has not been explored in this study, it could be cautiously suspected, as hinted from the KCC2 architecture studies (Agez et al., 2017), that the disulfide bond in the ECD which stabilizes its rigid

structure may play a role in the dimerization process (Liu et al., 2019). Note that the residues involved in the disulfide bond are highly conserved in both the KCC1 and KCC2 and mutations in these residues are known to abolish the activity of the KCC2 (Agez et al., 2017).

Lastly, the protein has 2 chloride ion binding sites and 1 potassium ion binding site (Liu et al., 2019). This is somewhat surprising given that the cotransporter transports the potassium and chloride at a 1:1 ratio. It is noted that one chloride ion is dependent on potassium in that the 3.6 Å distance allows two ions to be transported through interaction; the other chloride ion is independent of the potassium. In fact, it was shown that even in the absence of potassium (i.e. the protein in 150 mM NaCl), there was a presence of chloride ions in the second ion binding site. It is hypothesized that this binding is required for the stabilization of the binding site for K<sup>+</sup> that facilitates the coordination between the potassium and chloride. The binding of this chloride ion also further stabilizes the TM6a, TM6b, and TM10 during the ion transport process. From this, it could be deduced that Cl<sup>-</sup> binding alone is sufficient to stabilize the architecture for the protein and that potassium is not required. Because we wanted to limit the conformation of our KCC3 protein, we decided to purify and isolate our proteins using NaCl buffer without potassium.

### **Structural Analysis of Monomeric KCC4**

Reid et al. (2020) have published the 3-D high-resolution structure of the KCC4 through Cryo-EM. They solubilized the protein in 1% DDM and were reconstituted in MSPD1 nanodisc with a lipid mixture of 2:1:1 DOPE:POPS:POPC which is most reflective of the composition of the major neuronal membranes (Reid et al., 2020). In contrast to previous structures of NKCC1 and KCC1, as well as previous architecture and cross-linking studies of KCC2, KCC3, and KCC4,

the KCC4 structures presented here was in a monomer structure (Reid et al., 2020; Casula et al., 2009; Simard et al., 2007; Uvarov et al., 2007). The author reasoned that this is not due to the nanodisc reconstitution procedures as they were monomeric before and after the reconstitution (Reid et al., 2020). The author suggested that the extracellular loop of the KCC4, which played an important role in forming the dimer of the KCC1 (Liu et al., 2019), is sterically incompatible to form dimerization in KCC4 (Reid et al., 2020).

Regardless, the author still suspects that dimerization of the KCC4 may still occur and suggested in this work that monomeric and dimeric KCC4 may be functionally distinct; The author reasoned that its different oligomerization states may play a role in modulating the transporter activity.

Furthermore, the KCC4 structure published by Reid et al. (2020) was distinct from the KCC1 structure in that the second ion binding site for the chloride was observed in its structure. It is quite unclear why this may be the case, given that the mutation in the nearby tyrosine (Y466) reduces the activity of the KCC4 protein activity (Reid et al., 2020)

Regardless, this structure also further highlights the importance of preserving the disulfide bond of the protein for structural analysis. Disulfide bonds were, as presented in the KCC1 structure, presented between the C308-C323 and C343-C352 in the extracellular loop, as well as between C163(TM2)-C626(TM11) in the transmembrane region (Reid et al., 2020).

### **Structural Analysis of Dimeric KCC2, KCC3, and KCC4**

While our investigation was still being carried out in an attempt to find the high-resolution structure of the KCC3, Xie et al. (2021) was successfully able to obtain the cryo-EM

structure of not only KCC3 at 3.6 Å but also KCC2 and KCC4 (supplemental figure. 11). This was the first full-length structure of the WT KCC proteins, as previously published both KCC1 and KCC4 had C-terminus truncated (Liu et al., 2019; Reid et al., 2020).

As was previously predicted from multiple studies (Hartmann et al., 2015; Payne et al., 2012; Reid et al., 2020; Liu et al., 2019; Agez et al., 2017), all KCCs shared common structural features, such as extracellular domain characterized by the large loop between TM 5 and TM6 stabilized rigidly by the disulfide bonds, 12 transmembrane domain, intracellular CTD and NTD. Unlike the KCC4 that was published by Reid et al. (2020), the KCC4 structure published by Xie et al. (2021) was in the dimeric structure, indicating that previously published KCC4 may represent different oligomeric state. All KCC proteins also adopt a similar overall structure with a LeuT-like fold in the TMD and are captured in its inward-facing conformation. Like was observed in the KCC1 structure and was suggested in the KCC4 structure (Reid et al., 2020; Liu et al., 2019), two chloride ion binding sites and one potassium ion binding site was observed in all four proteins (Reid et al., 2020; Liu et al., 2019; Xie et al., 2020) (Supplemental figure 12.)

NTD seems to play an important role in inhibiting the function of the KCC proteins by blocking the intracellular solvent access to the ion-binding sites when it is at inward-facing conformation (Supplemental figure 13.) (Xie et al., 2020). Furthermore, Many single amino-acid substitution mutations in the conserved residues of the N-terminus (Y91A, T92E, N93A, L94A, Q96A, H101A) significantly increased the activity of the KCC2, it was suggested that N-terminus play an inhibitory role in nature (Xie et al., 2020). Lastly, the mutation of two acidic residues (E102A and E105A) in the KCC2 N-terminus that normally interact with the positive electrostatic surface of the CTD enhanced the KCC2, hinting that CTD may also play a stabilizing role in the inhibitory state of the KCC (Xie et al., 2020). It should be noted that CTD

is known to play a critical role in the activity of the transporter via phosphorylation (Ding et al., 2013; Lee et al., 2010; Kahle et al., 2016).

This structure also has highlighted the role of CTD that plays during the dimerization process that was not present in the previous studies. It was shown that CTD plays an important role in the dimerization process by the following hydrophobic interactions: 1) scissor helix in which L673, A675, A676, A679, L683 of the alpha strand from each peptide interact anti-parallelly; 2)  $\alpha$ 3- $\beta$ 3 linker interacting with the scissor helix via 786LGGL789; and 3) PI-PI interaction between two H779 residues of  $\alpha$ 3 (Supplemental figure 14.). Dimerization also occurred via hydrogen bond between S771 and Asp775 of the  $\beta$ 3- $\alpha$ 3 linker (Supplemental Figure 14.)

## **Conclusion**

Overall, this study illustrates the general molecular shape of the KCC3 protein and also describes the expression and purification of structurally intact KCC3 for cryo-EM studies. We also discuss some of the structural features of the KCC that we would have found if we were to obtain the high-resolution structure of our protein using previously published papers. Membrane protein has historically been challenging to study because of its hydrophobic transmembrane regions that are usually embedded in the lipid bilayer, which causes them to be very unstable and aggregate (Carpenter et al., 2008). This study can be used to serve as a groundwork for the expression and purification of other membrane proteins to discover their novel 3-D high-resolution structures. This work can also serve as a basis for other structural and functional investigations to elucidate the molecular mechanisms of not only the KCC3 proteins but also the other transmembrane proteins.

**Supplemental Tables****Table 1:** Table Summary of Purification Tags to Different Membrane Protein for Structural Studies

<b>Protein</b>	<b>Tag</b>
KCC1(Liu et al., 2019)	C-terminus <b>Strep tag</b>
Human NKCC1(Yang et al., 2020)	N-terminus <b>MBP tag</b>
Danio <i>Reiro</i> NKCC1(Chew et al., 2019)	N-terminus <b>MBP tag</b> + 3C Protease Site
KCC4(Reid et al., 2020)	C-terminus Precision protease site + linker sequence + sfGFP + <b>7x His tag</b>
KCC2 (for architecture study)(Agez et al., 2017)	Either <b>His-tag</b> or <b>Flag tag</b> or both in either terminus.
KCC2 (Xie et al., 2020)	N-terminal FLAG tag and C-terminal Strep tag II

KCC3 (Xie et al., 2020)	N-terminal FLAG tag and C-terminal Strep tag II
KCC4 (Xie et al., 2020)	N-terminal FLAG tag and C-terminal Strep tag II
Voltage-gated K <sup>+</sup> channel(Matthies et al., 2018)	N-terminus <b>10x His tag</b> + thrombin protease site
TPRV1(Liao et al., 2013)	N-terminus fusion cassette: Kozac- <b>MBP</b> -TEV protease site
NMDAR (GluN1-GluN2A-GluN2B)(Lu et al., 2017)	C-terminus eGFP+3C protease site + <b>8 histag</b> (GluN2B), C-terminus 3C protease cleavage site + eGFP + <b>StrepII tag</b> (GluN2A)
NMDAR (GluN1-GluN2B)(Zhu et al., 2016)	C-terminus 3C Protease site + eGFP tag + <b>8x his tag</b> (GluN1 subunit) or <b>Strep II tag</b> (GluN2B subunit)
AMPAR(Twomey et al., 2017)	C-terminus "Thr-Gly-Gly" + thrombin site +eGFT + <b>streptavin tag</b>
AMPAR(Zhao et al., 2019)	C-terminus <b>Strep II tag</b>
Calcium uniporter(Fan et al., 2018)	N-terminus <b>his tag</b> , GFP, 3C protease cleavage site

GABA <sub>A</sub> receptor(Zhu et al., 2018)	N-terminus <b>Twin Strep tag</b> (in the gamma-2 subunit)
GABA <sub>A</sub> receptor(Laverty et al., 2019)	N-terminus <b>Flag tag</b> (in alpha-1 subunit) and C-terminus <b>(GGG)3GK-1D4 tag</b> (in gamma-2 subunit)
GABA <sub>A</sub> receptor(Masiulis et al., 2019)	N-terminus <b>Flag tag</b> (alpha 1) + C-terminus <b>rhodopsin-1D4 tag</b> (gamma 2)
E.coli ATP synthase(Sobti et al., 2016)	N-terminus <b>6x his tag</b>
GPCR(Liang et al., 2017)	N-terminus <b>Flag tag</b> + C-terminus <b>6x his tag</b>
Rhodopsin(Kang et al., 2018)	N-terminus <b>8x his tag</b> + sfGFP + TEV site
SERT(Coleman et al., 2018)	C-terminus thrombin site + GFP + <b>twin strep tag</b> + <b>10x his tag</b>

**Table 2:** Table Summary of Buffer Conditions of Different KCC for Cryo-EM studies

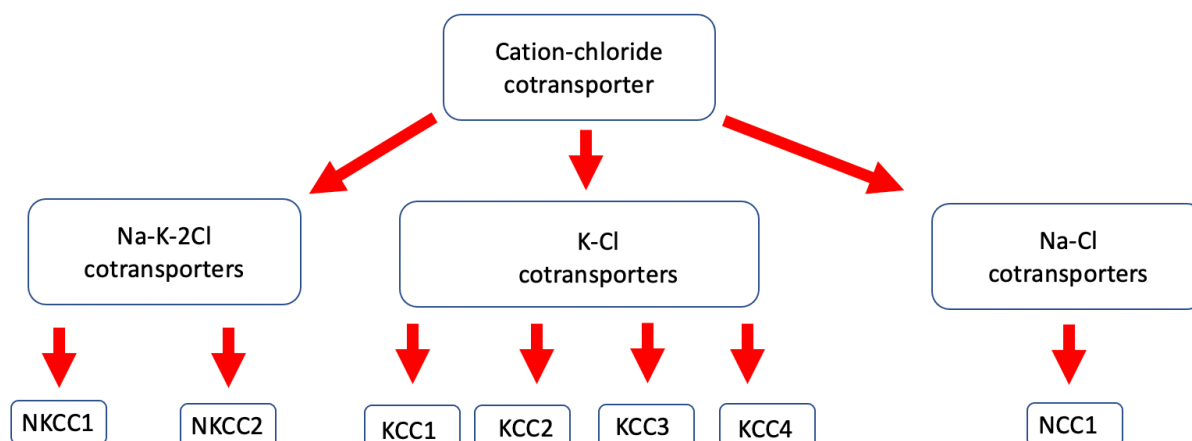
	Lysis	Wash	Elution	FPLC
--	-------	------	---------	------

KCC1 (Liu et al., 2019)	20 mM Tris pH 8.0, 150 mM KCl/NaCl, 2% DDM	20 mM Tris pH 8.0, 150 mM KCl/NaCl, 0.1% DDM	20 mM Tris pH 8.0, 150 mM KCl/NaCl, 0.06% GDN	20 mM Tris pH 8.0, 150 mM KCl/NaCl, 0.06% GDN
KCC4 (Reid et al., 2020)	50 mM Tris pH 8.0, 150 mM KCl, 1mM EDTA, 1% DDM	20 mM Tris pH 8.0, 150 mM/500 mM KCl, 1 mM EDTA, 0.025% DDM		20 mM Tris pH 8.0, 150 mM KCl, 1 mM EDTA, 0.025% DDM
drNKCC1 (Chew et al., 2019)	20 mM Tris-HCl, pH 8.0, 200 mM NaCl, 200 mM KCl, 1% LMNG	20 mM Tris-HCl, pH 8.0, 200 mM NaCl, 200 mM KCl	20 mM Tris-HCl, pH 8.0, 200 mM NaCl, 200 mM KCl, 0.06% digitonin	
hNKCC1 (Yang et al., 2020)	50 HEPES (pH 7.4), 150 NaCl, 0.5 TCEP, 0.5 MNG-3, 0.1 CHS, 1 MnCl <sub>2</sub> , 20 maltose, 0.1 mg/ml			20 HEPES (pH 7.4), 150 NaCl, 0.5 TCEP, $25 \times 10^{-3}$ MNG-3, and $5 \times 10^{-3}$ CHS

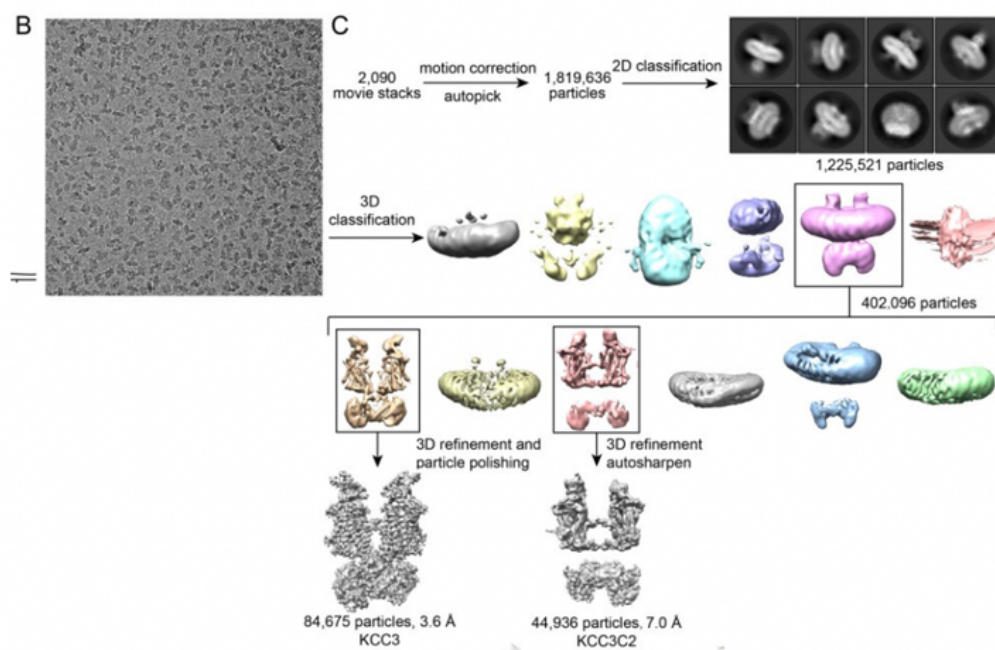
	soybean lipids, 10% glycerol			
KCC2,KCC3,KCC4 (Xie et al., 2020)	30 mM Tris pH 8.0, 150 mM KCl, 1% LMNG	30 mM Tris pH 8.0, 150 mM KCl, 0.005% LMNG	30 mM Tris pH 8.0, 150 mM KCl, 0.02% GDN	30 mM Tris pH 8.0, 150 mM KCl, 0.02% GDN

## Supplemental Figures

### SLC12 gene



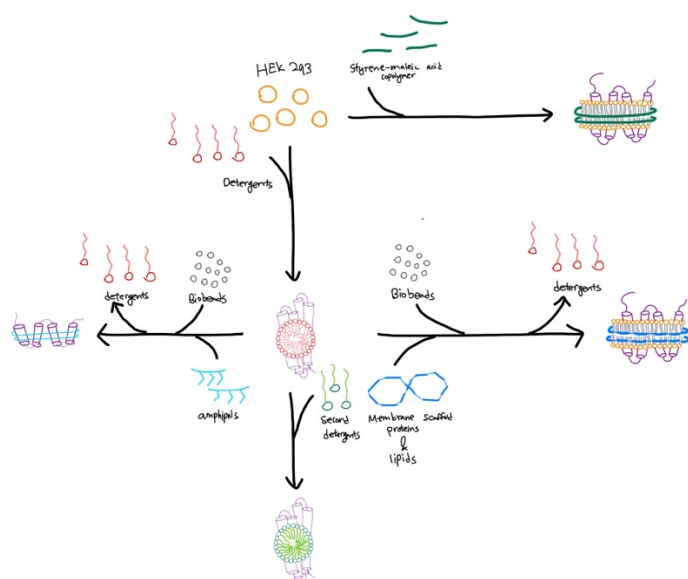
**Supplemental Figure 1: Proteins Encoded by SLC12 Gene**



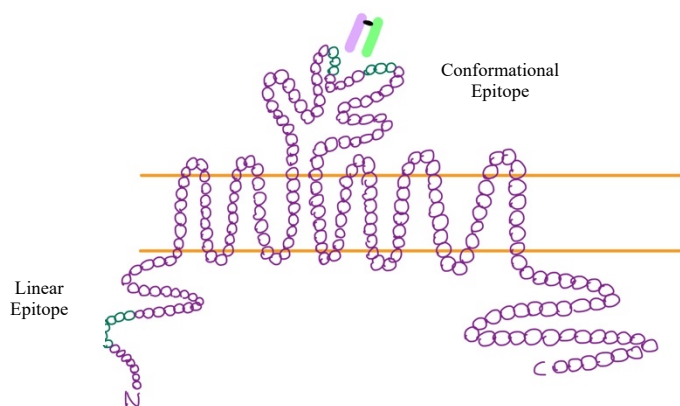
**Supplemental Figure 2: General Workflow of Cryo-EM Image processing (Xie et al., 2020)**

Reprinted Figures from Xie et al., *Science Advances* 11 Dec 2020:

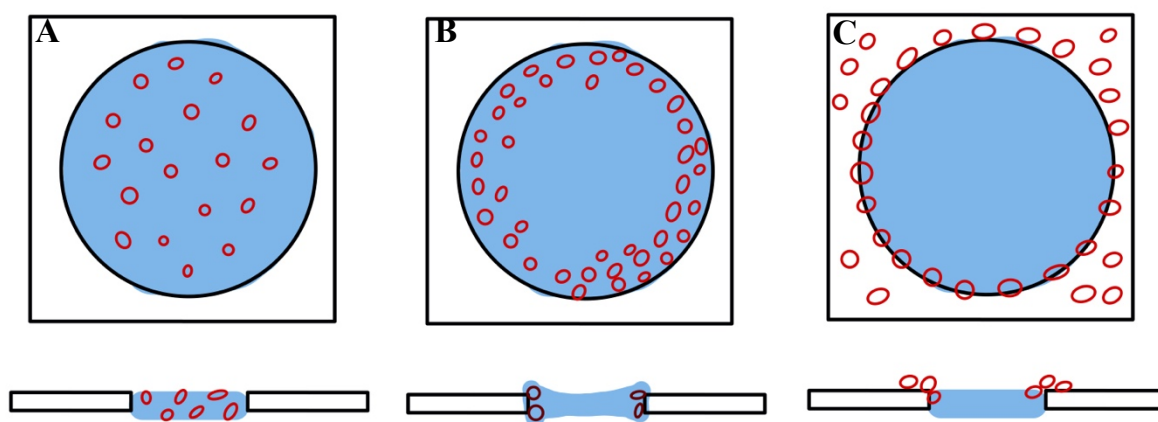
Vol. 6, no. 50, eabc5883 (DOI: 10.1126/sciadv.abc5883). © The Authors, some rights reserved;  
exclusive licensee AAAS. Distributed under a CC BY-NC 4.0 License  
(<http://creativecommons.org/licenses/by-nc/4.0/>)



**Supplemental Figure 3:** General Workflow of Membrane Protein Purification



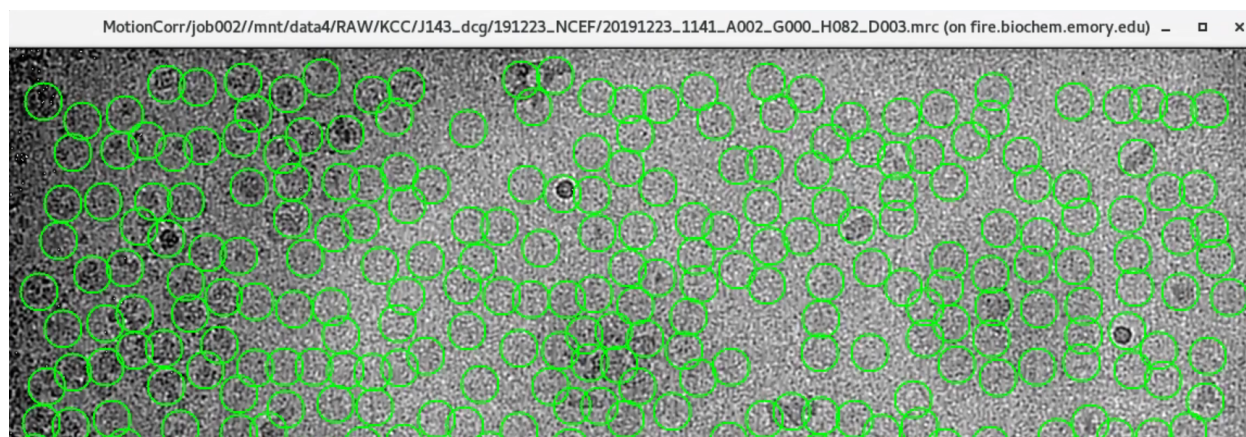
**Supplemental Figure 4:** Comparison Between Linear and Conformational Epitope



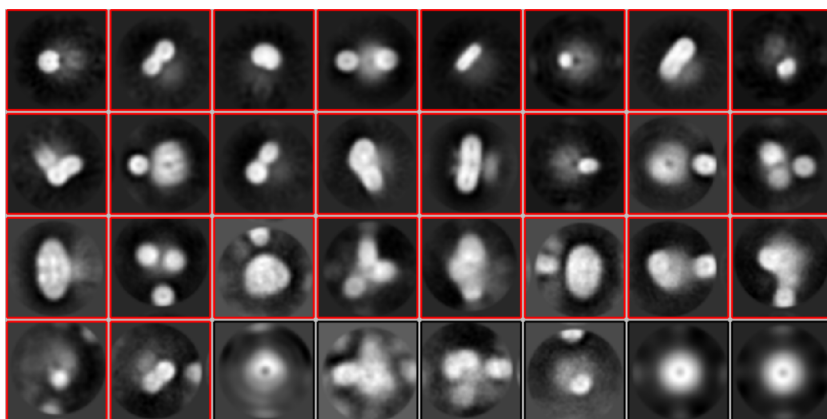
**Supplemental Figure 5:** Cartoon Representation of Protein in Cryo-EM Grids.

Top image corresponds to the top view of the grid holes. Bottom image is the side view of the grid holes. (A) represents the ideal cryo-grid samples with evenly distributed particles in the vitreous ice layer. (B) shows the thin ice layer in the center of the hole which may cause the

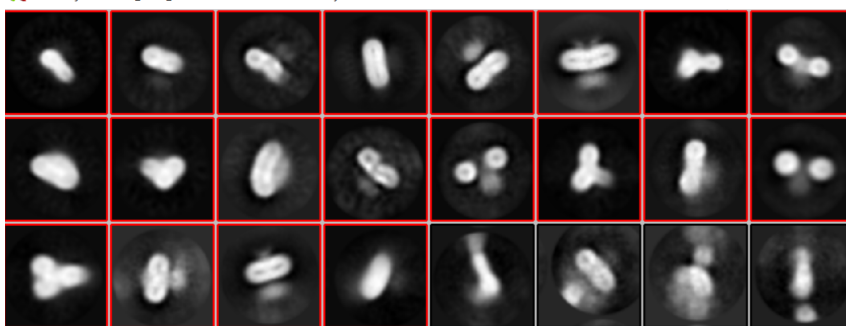
protein to get pushed towards the edge and aggregate. (C) shows that the particles have low affinity towards the center grid hole and is aggregated to the outer support layer.



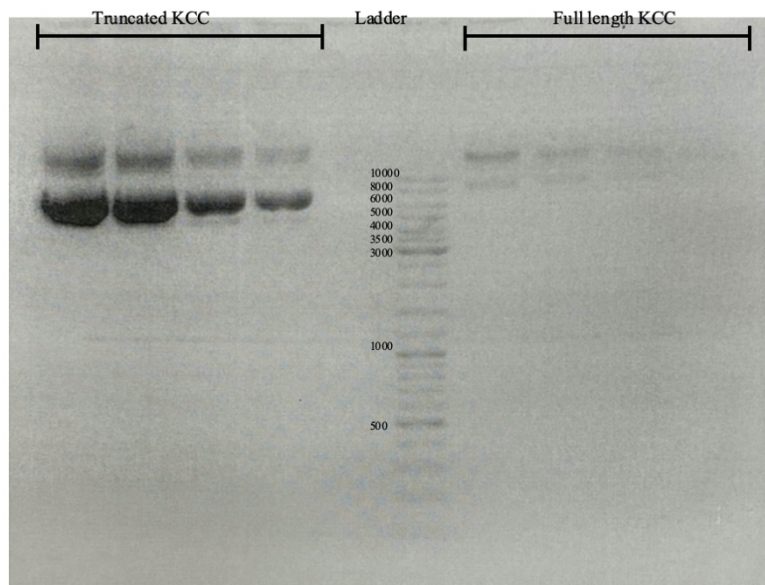
**Supplemental Figure 6:** Example Image of Particle Picking of Cryo Grid Images



X Class2D/job125/run\_it020\_model.star@fire.biochem.emory.edu

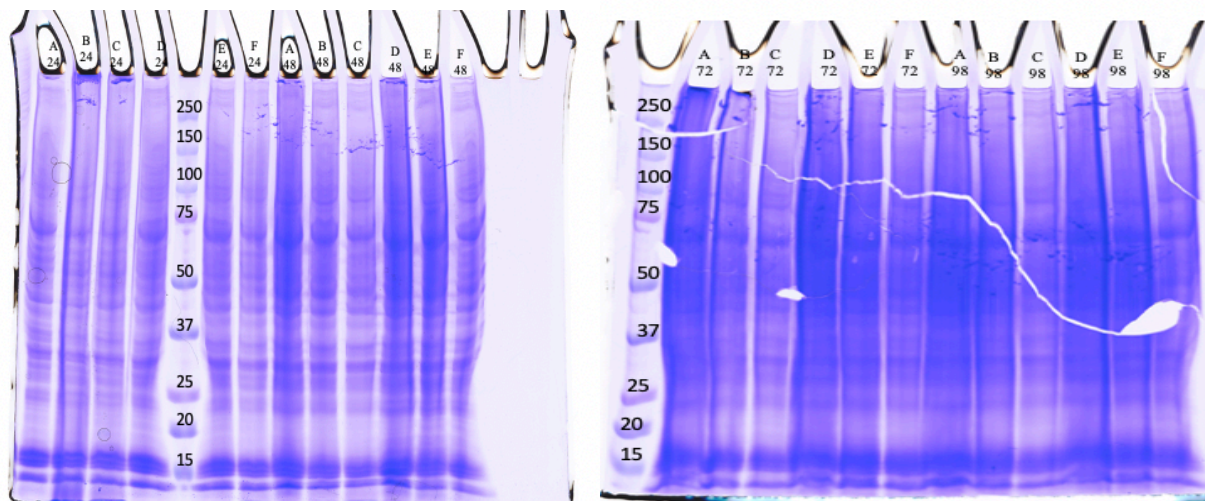


**Supplemental Figure 7: 2D Classifications of KCC3**



### Supplemental Figure 8: Gel Electrophoresis Image of the Plasmid

Image of gel electrophoresis of the circular plasmid after plasmid purification using Gigaprep kit (Qiagen) from the transformation of the newly synthesized KCC3 plasmid. Truncated KCC plasmid refers to the gene construct in which the gene responsible for expression of N-terminus of the KCC3 (1-109) has been truncated. Two bands exist for each plasmids because they were not linearized and the circular plasmid may form supercoiled conformation that runs faster in the gel than the open-circular plasmid. Regardless, the size of the bands for the full length KCC, as expected, are shown to be bigger than the truncated KCC and confirms that we were able to successfully purify our plasmid of interest.

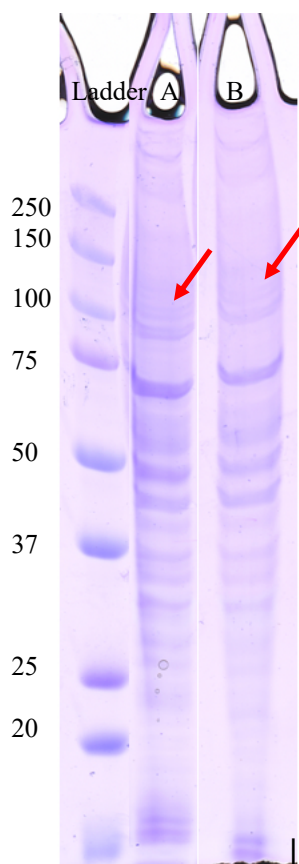


Label:

- A: 1.5 ug DNA/mL; 1:1.5 [DNA-PEI](#)
- B: 1.5 ug DNA/mL; 1:3 [DNA-PEI](#)
- C: 1.5 ug DNA/mL; 1:5 [DNA-PEI](#)
- D: 1.0 ug DNA/mL; 1:1.5 [DNA-PEI](#)
- E: 1.0 ug DNA/mL; 1:3 [DNA-PEI](#)
- F: 1.0 ug DNA/mL; 1:5 [DNA-PEI](#)

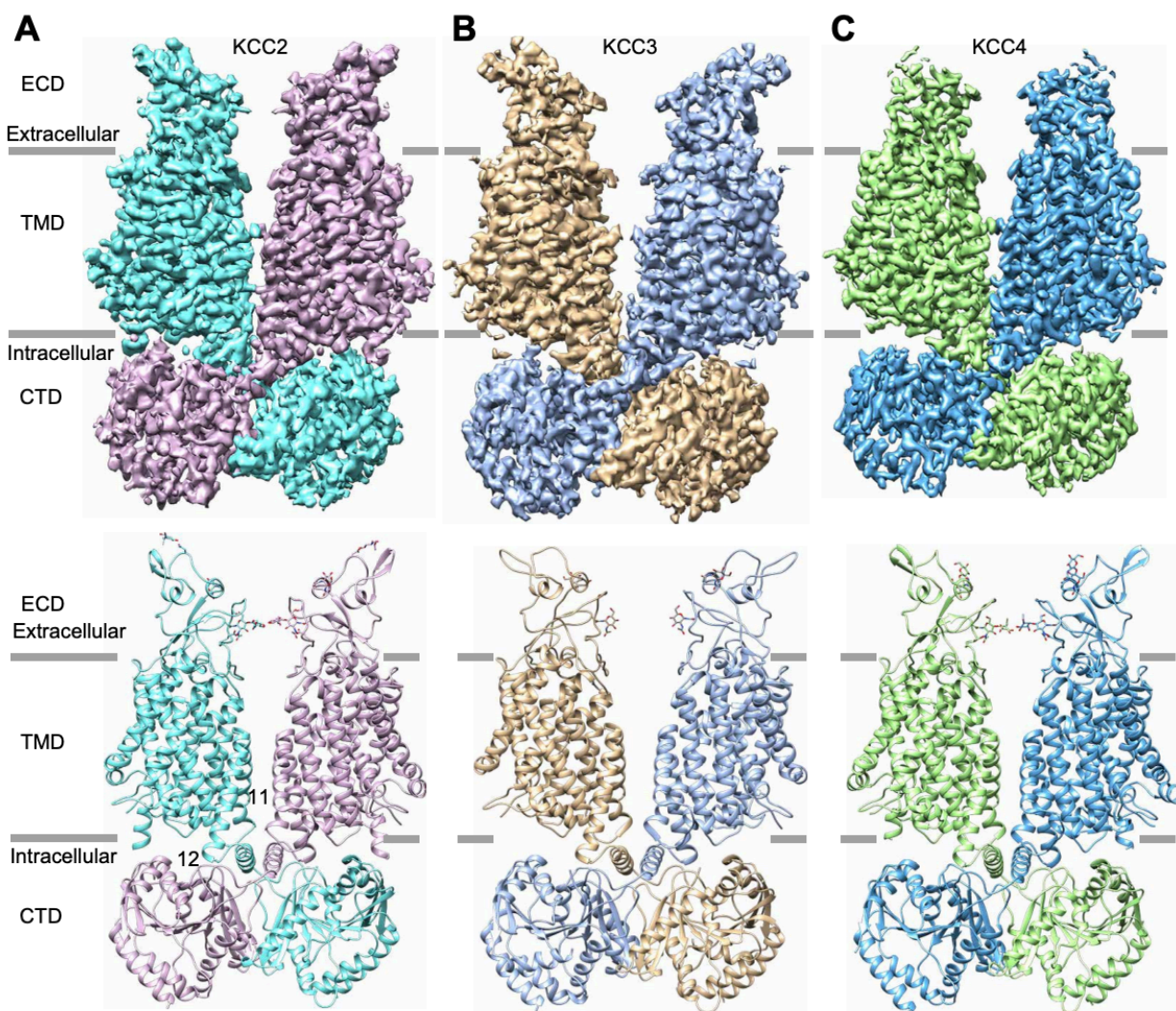
### Supplemental Figure 9: Small Volume Expression Test

Expression test of the whole cell extract after being transfected with the respective DNA:PEI ratio using PEI-based transfection method 1. The numbers represent the hours passed after the transfection. No bands were observed any of the samples, indicating that the PEI transfection method 1 may not be the most ideal transfection method to express our proteins.



**Supplemental Figure 10:** Small Volume Expression Test After VPA and SB

SDS page gel of the whole cell extract after being transfected with DNA:PEI ratio of 1:3 supplemented with 3 mM VPA post 3 hour transfection or 20 mM Sodium Butyrate post 24 hour transfection in 30°C.

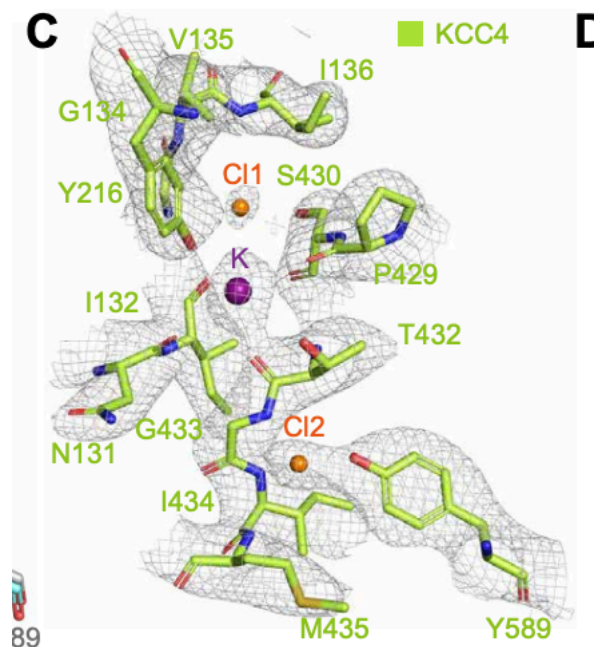


**Supplemental Figure 11:** Cryo-EM Images of Potassium-Chloride Cotransporters (Xie et al., 2020)

Reprinted Figures from Xie et al., *Science Advances* 11 Dec 2020:

Vol. 6, no. 50, eabc5883 (DOI: 10.1126/sciadv.abc5883). © The Authors, some rights reserved; exclusive licensee AAAS. Distributed under a CC BY-NC 4.0 License

(<http://creativecommons.org/licenses/by-nc/4.0/>)



**Supplemental Figure 12: Ion Binding Sites of KCC4** (Xie et al., 2020)

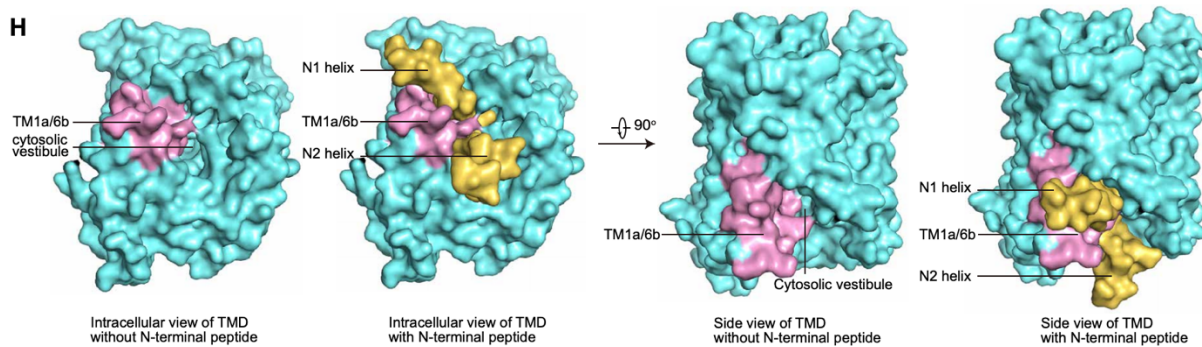
Electron densities indicating the two Cl<sup>-</sup> and one K<sup>+</sup> ion binding sites in KCC4.

Reprinted Figures from Xie et al., *Science Advances* 11 Dec 2020:

Vol. 6, no. 50, eabc5883 (DOI: 10.1126/sciadv.abc5883). © The Authors, some rights reserved;

exclusive licensee AAAS. Distributed under a CC BY-NC 4.0 License

(<http://creativecommons.org/licenses/by-nc/4.0/>)



**Supplemental Figure 13: N-terminal Peptide of KCC2 (Xie et al., 2020)**

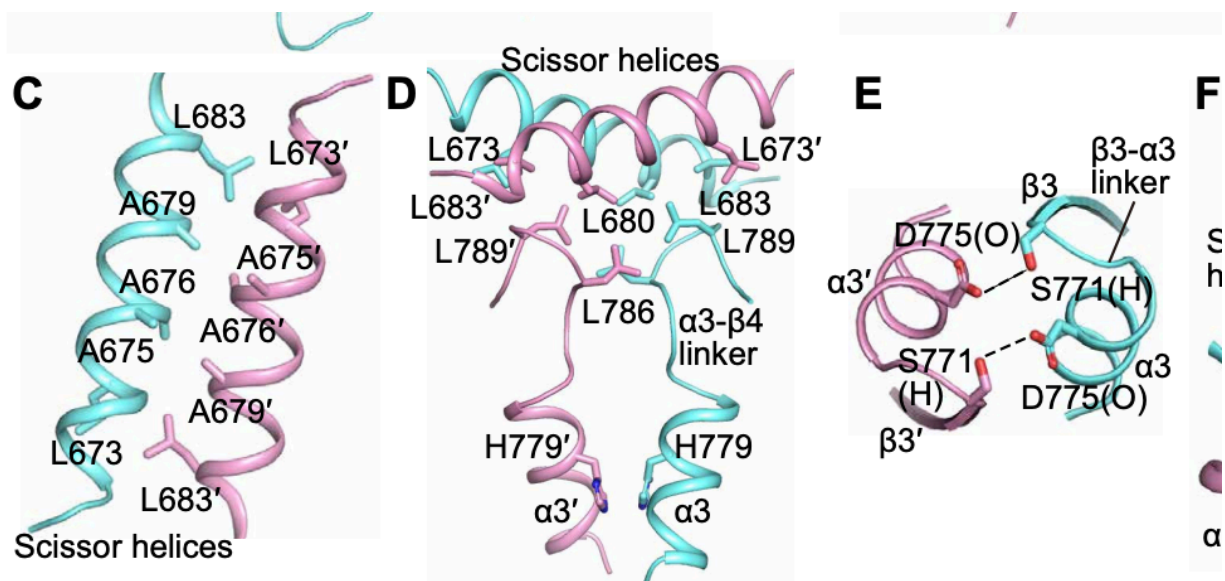
Visual representation of the NTD (yellow) in relation to the TMD (pink). It indicates that NTD blocks the access of intracellular solvent into the TM1a and TM6b where the substrate binding sites are.

Reprinted Figures from Xie et al., *Science Advances* 11 Dec 2020:

Vol. 6, no. 50, eabc5883 (DOI: 10.1126/sciadv.abc5883). © The Authors, some rights reserved;

exclusive licensee AAAS. Distributed under a CC BY-NC 4.0 License

(<http://creativecommons.org/licenses/by-nc/4.0/>)



**Supplemental Figure 14 : Hydrophobic Interactions Involved in KCC Dimerization**

Reprinted Figures from Xie et al., *Science Advances* 11 Dec 2020:

Vol. 6, no. 50, eabc5883 (DOI: 10.1126/sciadv.abc5883). © The Authors, some rights reserved;

exclusive licensee AAAS. Distributed under a CC BY-NC 4.0 License

(<http://creativecommons.org/licenses/by-nc/4.0/>)

**References:**

Agez, M., Schultz, P., Medina, I., Baker, D. J., Burnham, M. P., Cardarelli, R. A., Conway, L.

C., Garnier, K., Geschwindner, S., Gunnarsson, A., McCall, E. J., Frechard, A.,

Audebert, S., Deeb, T. Z., Moss, S. J., Brandon, N. J., Wang, Q., Dekker, N., & Jawhari,

A. (2017). Molecular architecture of potassium chloride co-transporter KCC2. *Scientific*

*Reports*. <https://doi.org/10.1038/s41598-017-15739-1>

Ansorge, S., Lanthier, S., Transfiguracion, J., Durocher, Y., Henry, O., & Kamen, A. (2009).

Development of a scalable process for high-yield lentiviral vector production by transient transfection of HEK293 suspension cultures. *Journal of Gene Medicine*.

<https://doi.org/10.1002/jgm.1370>

Aslan, H., Zilberman, Y., Arbeli, V., Sheyn, D., Matan, Y., Liebergall, M., Li, J. Z., Helm, G.

A., Gazit, D., & Gazit, Z. (2006). Nucleofection-based Ex vivo nonviral gene delivery to human stem cells as a platform for tissue regeneration. *Tissue Engineering*.

<https://doi.org/10.1089/ten.2006.12.877>

Autzen, H. E., Julius, D. & Cheng, Y. Membrane mimetic systems in CryoEM: keeping

membrane proteins in their native environment. *Current Opinion in Structural Biology*

(2019) doi:10.1016/j.sbi.2019.05.022.

Bayburt, T. H., Grinkova, Y. V. & Sligar, S. G. Self-Assembly of Discoidal Phospholipid

Bilayer Nanoparticles with Membrane Scaffold Proteins. *Nano Lett.* (2002)

doi:10.1021/nl025623k

Boettger, T., Rust, M. B., Maier, H., Seidenbecher, T., Schweizer, M., Keating, D. J., Faulhaber,

J., Ehmke, H., Pfeffer, C., Scheel, O., Lemcke, B., Horst, J., Leuwer, R., Pape, H. C.,

Völkl, H., Hübner, C. A., & Jentsch, T. J. (2003). Loss of K-Cl co-transporter KCC3

causes deafness, neurodegeneration and reduced seizure threshold. *EMBO Journal.*

<https://doi.org/10.1093/emboj/cdg519>

Boussif, O., LezoualC'H, F., Zanta, M. A., Mergny, M. D., Scherman, D., Demeneix, B., &

Behr, J. P. (1995). A versatile vector for gene and oligonucleotide transfer into cells in

culture and in vivo: Polyethylenimine. *Proceedings of the National Academy of Sciences*

*of the United States of America.* <https://doi.org/10.1073/pnas.92.16.7297>

Bowerman, M., Salsac, C., Bernard, V., Soulard, C., Dionne, A., Coque, E., Benlefki, S., Hince,

P., Dion, P. A., Butler-Browne, G., Camu, W., Bouchard, J. P., Delpire, E., Rouleau, G.

A., Raoul, C., & Scamps, F. (2017). KCC3 loss-of-function contributes to Andermann

syndrome by inducing activity-dependent neuromuscular junction defects. *Neurobiology*

*of Disease.* <https://doi.org/10.1016/j.nbd.2017.06.013>

Burgess, R. R. (1991). Use of Polyethyleneimine in Purification of DNA-Binding Proteins.

*Methods in Enzymology.* [https://doi.org/10.1016/0076-6879\(91\)08003-Z](https://doi.org/10.1016/0076-6879(91)08003-Z)

Byun, N., & Delpire, E. (2007). Axonal and periaxonal swelling precede peripheral

neurodegeneration in KCC3 knockout mice. *Neurobiology of Disease*.

<https://doi.org/10.1016/j.nbd.2007.06.014>

Carpenter, E. P., Beis, K., Cameron, A. D., & Iwata, S. (2008). Overcoming the challenges of

membrane protein crystallography. In *Current Opinion in Structural Biology*.

<https://doi.org/10.1016/j.sbi.2008.07.001>

Casula, S., Zolotarev, A. S., Stuart-Tilley, A. K., Wilhelm, S., Shmukler, B. E., Brugnara, C., &

Alper, S. L. (2009). Chemical crosslinking studies with the mouse Kcc1 K-Cl cotransporter. *Blood Cells, Molecules, and Diseases*.

<https://doi.org/10.1016/j.bcmed.2009.01.021>

Cervera, L., Fuenmayor, J., González-Domínguez, I., Gutiérrez-Granados, S., Segura, M. M., &

Gòdia, F. (2015). Selection and optimization of transfection enhancer additives for increased virus-like particle production in HEK293 suspension cell cultures. *Applied Microbiology and Biotechnology*. <https://doi.org/10.1007/s00253-015-6842-4>

Chae, P. S., Rasmussen, S. G. F., Rana, R. R., Gotfryd, K., Kruse, A. C., Manglik, A., Cho, K.

H., Nurva, S., Gether, U., Guan, L., Loland, C. J., Byrne, B., Kobilka, B. K., & Gellman, S. H. (2012). A new class of amphiphiles bearing rigid hydrophobic groups for solubilization and stabilization of membrane proteins. *Chemistry - A European Journal*.

<https://doi.org/10.1002/chem.201200069>

Chen, B., Li, Y., Yu, B., Zhang, Z., Brommer, B., Williams, P. R., Liu, Y., Hegarty, S. V., Zhou,

- S., Zhu, J., Guo, H., Lu, Y., Zhang, Y., Gu, X., & He, Z. (2018). Reactivation of Dormant Relay Pathways in Injured Spinal Cord by KCC2 Manipulations. *Cell*.  
<https://doi.org/10.1016/j.cell.2018.06.005>
- Chew, T. A., Orlando, B. J., Zhang, J., Latorraca, N. R., Wang, A., Hollingsworth, S. A., Chen, D. H., Dror, R. O., Liao, M., & Feng, L. (2019). Structure and mechanism of the cation–chloride cotransporter NKCC1. *Nature*. <https://doi.org/10.1038/s41586-019-1438-2>
- Choy, B. C., Cater, R. J., Mancina, F., & Pryor, E. E. (2021). A 10-year meta-analysis of membrane protein structural biology: Detergents, membrane mimetics, and structure determination techniques. *Biochimica et Biophysica Acta - Biomembranes*.  
<https://doi.org/10.1016/j.bbamem.2020.183533>
- Coleman, J. A., & Gouaux, E. (2018). Structural basis for recognition of diverse antidepressants by the human serotonin transporter. *Nature Structural and Molecular Biology*.  
<https://doi.org/10.1038/s41594-018-0026-8>
- Collins, P. L., Hill, M. G., Cristina, J., & Grosfeld, H. (1996). Transcription elongation factor of respiratory syncytial virus, a nonsegmented negative-strand RNA virus. *Proceedings of the National Academy of Sciences of the United States of America*.  
<https://doi.org/10.1073/pnas.93.1.81>

Cowton, V. M., McGivern, D. R., & Fearn, R. (2006). Unravelling the complexities of respiratory syncytial virus RNA synthesis. In *Journal of General Virology*.

<https://doi.org/10.1099/vir.0.81786-0>

Delpire, E., & Weaver, C. D. (2016). Challenges of Finding Novel Drugs Targeting the K-Cl Cotransporter. *ACS Chemical Neuroscience*.

<https://doi.org/10.1021/acschemneuro.6b00366>

Ding, J., Ponce-Coria, J., & Delpire, E. (2013). A Trafficking-Deficient Mutant of KCC3 Reveals Dominant-Negative Effects on K-Cl Cotransport Function. *PLoS ONE*.

<https://doi.org/10.1371/journal.pone.0061112>

Dörr, J. M., Scheidelaar, S., Koorengel, M. C., Dominguez, J. J., Schäfer, M., van Walree, C.

A., & Killian, J. A. (2016). The styrene–maleic acid copolymer: a versatile tool in membrane research. In *European Biophysics Journal*. <https://doi.org/10.1007/s00249-015-1093-y>

Drulyte, I., Johnson, R. M., Hesketh, E. L., Hurdiss, D. L., Scarff, C. A., Porav, S. A., Ranson,

N. A., Muench, S. P., & Thompson, R. F. (2018). Approaches to altering particle distributions in cryo-electron microscopy sample preparation. *Acta Crystallographica Section D: Structural Biology*. <https://doi.org/10.1107/S2059798318006496>

Fan, C., Fan, M., Orlando, B. J., Fastman, N. M., Zhang, J., Xu, Y., Chambers, M. G., Xu, X.,

- Perry, K., Liao, M., & Feng, L. (2018). X-ray and cryo-EM structures of the mitochondrial calcium uniporter. *Nature*. <https://doi.org/10.1038/s41586-018-0330-9>
- Fan, S., Maguire, C. A., Ramirez, S. H., Bradel-Tretheway, B., Sapinoro, R., Sui, Z., Chakraborty-Sett, S., & Dewhurst, S. (2005). Valproic acid enhances gene expression from viral gene transfer vectors. *Journal of Virological Methods*. <https://doi.org/10.1016/j.jviromet.2004.11.023>
- Flores, B., Schornak, C. C., & Delpire, E. (2019). A role for KCC3 in maintaining cell volume of peripheral nerve fibers. In *Neurochemistry International*. <https://doi.org/10.1016/j.neuint.2018.01.009>
- Flores, B., Schornak, C. C., & Delpire, E. (2019). A role for KCC3 in maintaining cell volume of peripheral nerve fibers. In *Neurochemistry International*. <https://doi.org/10.1016/j.neuint.2018.01.009>
- Frank, J. (2002). Single-particle imaging of macromolecules by cryo-electron microscopy. In *Annual Review of Biophysics and Biomolecular Structure*. <https://doi.org/10.1146/annurev.biophys.31.082901.134202>
- Gamba, G. (2005). Molecular physiology and pathophysiology of electroneutral cation-chloride cotransporters. In *Physiological Reviews*. <https://doi.org/10.1152/physrev.00011.2004>
- Gao, Y., Cao, D., Ahn, H. M., Swain, A., Hill, S., Ogilvie, C., Kurien, M., Rahmatullah, T., &

- Liang, B. (2020). In vitro trackable assembly of RNA-specific nucleocapsids of the respiratory syncytial virus. *Journal of Biological Chemistry*.  
<https://doi.org/10.1074/jbc.RA119.011602>
- Gao, Y., Cao, D., Pawnikar, S., John, K. P., Ahn, H. M., Hill, S., Ha, J. M., Parikh, P., Ogilvie, C., Swain, A., Yang, A., Bell, A., Salazar, A., Miao, Y., & Liang, B. (2020). Structure of the Human Respiratory Syncytial Virus M2-1 Protein in Complex with a Short Positive-Sense Gene-End RNA. *Structure*. <https://doi.org/10.1016/j.str.2020.07.001>
- Garneau, A. P., Marcoux, A. A., Noël, M., Frenette-Cotton, R., Drolet, M. C., Couet, J., Larivière, R., & Isenring, P. (2016). Ablation of potassium-chloride cotransporter type 3 (Kcc3) in mouse causes multiple cardiovascular defects and isosmotic polyuria. *PLoS ONE*. <https://doi.org/10.1371/journal.pone.0154398>
- Hartmann, A. M., & Nothwang, H. G. (2015). Molecular and evolutionary insights into the structural organization of cation chloride cotransporters. *Frontiers in Cellular Neuroscience*. <https://doi.org/10.3389/fncel.2014.00470>
- Howard, H. C., Mount, D. B., Rochefort, D., Byun, N., Dupré, N., Lu, J., Fan, X., Song, L., Rivière, J. B., Prévost, C., Horst, J., Simonati, A., Lemcke, B., Welch, R., England, R., Zhan, F. Q., Mercado, A., Siesser, W. B., George, A. L., ... Rouleau, G. A. (2002). The K-Cl cotransporter KCC3 is mutant in a severe peripheral neuropathy associated with agenesis of the corpus callosum. *Nature Genetics*. <https://doi.org/10.1038/ng1002>

Hu, J., Qin, H., Gao, F. P., & Cross, T. A. (2011). A systematic assessment of mature MBP in

membrane protein production: Overexpression, membrane targeting and purification.

*Protein Expression and Purification*. <https://doi.org/10.1016/j.pep.2011.06.001>

Joiner, C. H., Rettig, R. K., Jiang, M. & Franco, R. S. KCl cotransport mediates abnormal

sulfhydryl-dependent volume regulation in sickle reticulocytes. *Blood* (2004)

doi:10.1182/blood2004-01-0112.

Kahle, K. T., Flores, B., Bharucha-Goebel, D., Zhang, J., Donkervoort, S., Hegde, M., Hussain,

G., Duran, D., Liang, B., Sun, D., Bönnemann, C. G., & Delpire, E. (2016). Peripheral motor neuropathy is associated with defective kinase regulation of the KCC3

cotransporter. *Science Signaling*. <https://doi.org/10.1126/scisignal.aae0546>

Kahle, K. T., Flores, B., Bharucha-Goebel, D., Zhang, J., Donkervoort, S., Hegde, M., Hussain,

G., Duran, D., Liang, B., Sun, D., Bönnemann, C. G., & Delpire, E. (2016). Peripheral motor neuropathy is associated with defective kinase regulation of the KCC3

cotransporter. *Science Signaling*. <https://doi.org/10.1126/scisignal.aae0546>

Kahle, K. T., Merner, N. D., Friedel, P., Silayeva, L., Liang, B., Khanna, A., Shang, Y.,

Lachance-Touchette, P., Bourassa, C., Levert, A., Dion, P. A., Walcott, B., Spiegelman, D., Dionne-Laporte, A., Hodgkinson, A., Awadalla, P., Nikbakht, H., Majewski, J.,

Cossette, P., ... Rouleau, G. A. (2014). Genetically encoded impairment of neuronal

KCC 2 cotransporter function in human idiopathic generalized epilepsy . *EMBO Reports*.

<https://doi.org/10.15252/embr.201438840>

Kang, Y., Kuybeda, O., De Waal, P. W., Mukherjee, S., Van Eps, N., Dutka, P., Zhou, X. E.,

Bartesaghi, A., Erramilli, S., Morizumi, T., Gu, X., Yin, Y., Liu, P., Jiang, Y., Meng, X.,

Zhao, G., Melcher, K., Ernst, O. P., Kossiakoff, A. A., ... Xu, H. E. (2018). Cryo-EM

structure of human rhodopsin bound to an inhibitory G protein. *Nature*.

<https://doi.org/10.1038/s41586-018-0215-y>

Laverty, D., Desai, R., Uchański, T., Masiulis, S., Stec, W. J., Malinauskas, T., Zivanov, J.,

Pardon, E., Steyaert, J., Miller, K. W., & Aricescu, A. R. (2019). Cryo-EM structure of the human  $\alpha 1\beta 3\gamma 2$  GABAA receptor in a lipid bilayer. *Nature*.

<https://doi.org/10.1038/s41586-018-0833-4>

Le Bon, C., Marconnet, A., Masscheleyn, S., Popot, J. L., & Zoonens, M. (2018). Folding and

stabilizing membrane proteins in amphipol A8-35. In *Methods*.

<https://doi.org/10.1016/j.ymeth.2018.04.012>

Lee, H. H. C., Jurd, R., & Moss, S. J. (2010). Tyrosine phosphorylation regulates the membrane

trafficking of the potassium chloride co-transporter KCC2. *Molecular and Cellular*

*Neuroscience*. <https://doi.org/10.1016/j.mcn.2010.06.008>

Li, L., Sun, Y., Liu, J., Wu, X., Chen, L., Ma, L., & Wu, P. (2015). Histone deacetylase inhibitor

sodium butyrate suppresses DNA double strand break repair induced by etoposide more effectively in MCF-7 cells than in HEK293 cells. *BMC Biochemistry*.

<https://doi.org/10.1186/s12858-014-0030-5>

Liang, Y. L., Khoshouei, M., Radjainia, M., Zhang, Y., Glukhova, A., Tarrasch, J., Thal, D. M.,

Furness, S. G. B., Christopoulos, G., Coudrat, T., Danev, R., Baumeister, W., Miller, L.

J., Christopoulos, A., Kobilka, B. K., Wootten, D., Skiniotis, G., & Sexton, P. M. (2017).

Phase-plate cryo-EM structure of a class B GPCR-G-protein complex. *Nature*.

<https://doi.org/10.1038/nature22327>

Liao, M., Cao, E., Julius, D. & Cheng, Y. Single particle electron cryo-microscopy of a

mammalian ion channel. *Current Opinion in Structural Biology* (2014)

doi:10.1016/j.sbi.2014.02.005.

Liao, M., Cao, E., Julius, D., & Cheng, Y. (2013). Structure of the TRPV1 ion channel

determined by electron cryo-microscopy. *Nature*. <https://doi.org/10.1038/nature12822>

Lin, C. Y., Huang, Z., Wen, W., Wu, A., Wang, C., & Niu, L. (2015). Enhancing protein

expression in HEK-293 cells by lowering culture temperature. *PLoS ONE*.

<https://doi.org/10.1371/journal.pone.0123562>

Liu, S., Chang, S., Han, B., Xu, L., Zhang, M., Zhao, C., Yang, W., Wang, F., Li, J., Delpire, E.,

- Ye, S., Bai, X. C., & Guo, J. (2019). Cryo-EM structures of the human cation-chloride cotransporter KCC1. *Science*. <https://doi.org/10.1126/science.aay3129>
- Liu, S., Chang, S., Han, B., Xu, L., Zhang, M., Zhao, C., Yang, W., Wang, F., Li, J., Delpire, E., Ye, S., Bai, X. C., & Guo, J. (2019). Cryo-EM structures of the human cation-chloride cotransporter KCC1. *Science*. <https://doi.org/10.1126/science.aay3129>
- Longo, P. A., Kavran, J. M., Kim, M. S., & Leahy, D. J. (2013). Transient mammalian cell transfection with polyethylenimine (PEI). In *Methods in Enzymology*. <https://doi.org/10.1016/B978-0-12-418687-3.00018-5>
- Longo, P. A., Kavran, J. M., Kim, M. S., & Leahy, D. J. (2013). Transient mammalian cell transfection with polyethylenimine (PEI). In *Methods in Enzymology*. <https://doi.org/10.1016/B978-0-12-418687-3.00018-5>
- Lü, W., Du, J., Goehring, A., & Gouaux, E. (2017). Cryo-EM structures of the triheteromeric NMDA receptor and its allosteric modulation. *Science*. <https://doi.org/10.1126/science.aal3729>
- Marchion, D. C., Bicaku, E., Daud, A. I., Sullivan, D. M., & Munster, P. N. (2005). Valproic acid alters chromatin structure by regulation of chromatin modulation proteins. *Cancer Research*. <https://doi.org/10.1158/0008-5472.CAN-04-2478>
- Masiulis, S., Desai, R., Uchański, T., Serna Martin, I., Lavery, D., Karia, D., Malinauskas, T.,

- Zivanov, J., Pardon, E., Kotecha, A., Steyaert, J., Miller, K. W., & Aricescu, A. R. (2019). GABAA receptor signalling mechanisms revealed by structural pharmacology. *Nature*. <https://doi.org/10.1038/s41586-018-0832-5>
- Matthies, D., Bae, C., Toombes, G. E. S., Fox, T., Bartesaghi, A., Subramaniam, S., & Swartz, K. J. (2018). Single-particle cryo-EM structure of a voltage-activated potassium channel in lipid nanodiscs. *ELife*. <https://doi.org/10.7554/eLife.37558>
- Mercado, A., Broumand, V., Zandi-Nejad, K., Enck, A. H., & Mount, D. B. (2006). A C-terminal domain in KCC2 confers constitutive K<sup>+</sup>-Cl<sup>-</sup> cotransport. *Journal of Biological Chemistry*. <https://doi.org/10.1074/jbc.M509972200>
- Mount, D. B., Mercado, A., Song, L., Jason, X., George, A. L., Delpire, E., & Gamba, G. (1999). Cloning and characterization of KCC3 and KCC4, new members of the cation-chloride cotransporter gene family. *Journal of Biological Chemistry*. <https://doi.org/10.1074/jbc.274.23.16355>
- Orlov, S. N., Koltsova, S. V., Kapilevich, L. V., Dulin, N. O., & Gusakova, S. V. (2014). Cation-chloride cotransporters: Regulation, physiological significance, and role in pathogenesis of arterial hypertension. In *Biochemistry (Moscow)*. <https://doi.org/10.1134/S0006297914130070>
- Park, J., Flores, B. R., Scherer, K., Kuepper, H., Rossi, M., Rupprich, K., Rautenberg, M.,

- Deininger, N., Weichselbaum, A., Grimm, A., Sturm, M., Grasshoff, U., Delpire, E., & Haack, T. B. (2020). De novo variants in SLC12A6 cause sporadic early-onset progressive sensorimotor neuropathy. *Journal of Medical Genetics*.  
<https://doi.org/10.1136/jmedgenet-2019-106273>
- Payne, J. A. (2012). Molecular Operation of the Cation Chloride Cotransporters: Ion Binding and Inhibitor Interaction. In *Current Topics in Membranes*. <https://doi.org/10.1016/B978-0-12-394316-3.00006-5>
- Pearson, M. M., Lu, J., Mount, D. B., & Delpire, E. (2001). Localization of the K<sup>+</sup>-Cl<sup>-</sup> cotransporter, KCC3, in the central and peripheral nervous systems: Expression in the choroid plexus, large neurons and white matter tracts. *Neuroscience*.  
[https://doi.org/10.1016/S0306-4522\(00\)00567-4](https://doi.org/10.1016/S0306-4522(00)00567-4)
- Pearson, M. M., Lu, J., Mount, D. B., & Delpire, E. (2001). Localization of the K<sup>+</sup>-Cl<sup>-</sup> cotransporter, KCC3, in the central and peripheral nervous systems: Expression in the choroid plexus, large neurons and white matter tracts. *Neuroscience*.  
[https://doi.org/10.1016/S0306-4522\(00\)00567-4](https://doi.org/10.1016/S0306-4522(00)00567-4)
- Portolano, N., Watson, P. J., Fairall, L., Millard, C. J., Milano, C. P., Song, Y., Cowley, S. M., & Schwabe, J. W. R. (2014). Recombinant protein expression for structural biology in HEK 293F suspension cells: A novel and accessible approach. *Journal of Visualized Experiments*. <https://doi.org/10.3791/51897>

Reid, M. S., Kern, D. M., & Brohawn, S. G. (2020). Cryo-EM structure of the potassium-chloride cotransporter KCC4 in lipid nanodiscs. *ELife*.

<https://doi.org/10.7554/eLife.52505>

Schlaeger, E. J., & Lundstrom, K. (1998). Effect of temperature on recombinant protein expression in Semliki Forest virus infected mammalian cell lines growing in serum-free suspension cultures. *Cytotechnology*. <https://doi.org/10.1023/a:1008006504379>

Schnepf, B. C., Clark, K. R., Klemanski, D. L., Pacak, C. A., & Johnson, P. R. (2003). Genetic Fate of Recombinant Adeno-Associated Virus Vector Genomes in Muscle. *Journal of Virology*. <https://doi.org/10.1128/jvi.77.6.3495-3504.2003>

Serna, M. (2019). Hands on methods for high resolution cryo-electron microscopy structures of heterogeneous macromolecular complexes. In *Frontiers in Molecular Biosciences*. <https://doi.org/10.3389/fmolb.2019.00033>

Sgro, G. G., & Costa, T. R. D. (2018). Cryo-EM Grid Preparation of Membrane Protein Samples for Single Particle Analysis. *Frontiers in Molecular Biosciences*. <https://doi.org/10.3389/fmolb.2018.00074>

Simard, C. F., Bergeron, M. J., Frenette-Cotton, R., Carpentier, G. A., Pelchat, M. E., Caron, L.,

- & Isenring, P. (2007). Homooligomeric and heterooligomeric associations between K<sup>+</sup>-Cl<sup>-</sup> cotransporter isoforms and between K<sup>+</sup>-Cl<sup>-</sup> and Na<sup>+</sup>-K<sup>+</sup>-Cl<sup>-</sup> cotransporters. *Journal of Biological Chemistry*. <https://doi.org/10.1074/jbc.M607811200>
- Sobti, M., Smits, C., Wong, A. S. W., Ishmukhametov, R., Stock, D., Sandin, S., & Stewart, A. G. (2016). Cryo-EM structures of the autoinhibited E. coli ATP synthase in three rotational states. *ELife*. <https://doi.org/10.7554/eLife.21598>
- Sonawane, N. D., Szoka, F. C., & Verkman, A. S. (2003). Chloride Accumulation and Swelling in Endosomes Enhances DNA Transfer by Polyamine-DNA Polyplexes. *Journal of Biological Chemistry*. <https://doi.org/10.1074/jbc.M308643200>
- Stöberg, T., McTague, A., Ruiz, A. J., Hirata, H., Zhen, J., Long, P., Farabella, I., Meyer, E., Kawahara, A., Vassallo, G., Stivaros, S. M., Bjursell, M. K., Stranneheim, H., Tigerschiöld, S., Persson, B., Bangash, I., Das, K., Hughes, D., Lesko, N., ... Kurian, M. A. (2015). Mutations in SLC12A5 in epilepsy of infancy with migrating focal seizures. *Nature Communications*. <https://doi.org/10.1038/ncomms9038>
- Subedi, G. P., Johnson, R. W., Moniz, H. A., Moremen, K. W., & Barb, A. (2015). High yield expression of recombinant human proteins with the transient transfection of HEK293 cells in suspension. *Journal of Visualized Experiments*. <https://doi.org/10.3791/53568>
- Thompson, S. M., Deisz, R. A., & Prince, D. A. (1988). Outward chloride/cation co-transport in

mammalian cortical neurons. *Neuroscience Letters*. [https://doi.org/10.1016/0304-3940\(88\)90479-X](https://doi.org/10.1016/0304-3940(88)90479-X)

Twomey, E. C., Yelshanskaya, M. V., Grassucci, R. A., Frank, J., & Sobolevsky, A. I. (2017).

Channel opening and gating mechanism in AMPA-subtype glutamate receptors. *Nature*.  
<https://doi.org/10.1038/nature23479>

Ullah, R., Ali Shah, M., Tufail, S., Ismat, F., Imran, M., Iqbal, M., Mirza, O., & Rhaman, M.

(2016). Activity of the Human Rhinovirus 3C Protease Studied in Various Buffers, Additives and Detergents Solutions for Recombinant Protein Production. *PLoS ONE*.  
<https://doi.org/10.1371/journal.pone.0153436>

Uvarov, P. *et al.* A novel N-terminal isoform of the neuron-specific K-Cl cotransporter KCC2. *J.*

*Biol. Chem.* (2007) doi:10.1074/jbc.M705095200

Uyanik, G., Elcioglu, N., Penzien, J., Gross, C., Yilmaz, Y., Olmez, A., Demir, E., Wahl, D.,

Scheglmann, K., Winner, B., Bogdahn, U., Topaloglu, H., Hehr, U., & Winkler, J.

(2006). Novel truncating and missense mutations of the KCC3 gene associated with Andermann syndrome. *Neurology*. <https://doi.org/10.1212/01.wnl.0000204181.31175.8b>

Walz, W., & Hertz, L. (1984). Intense furosemide-sensitive potassium accumulation in

astrocytes in the presence of pathologically high extracellular potassium levels. *Journal of Cerebral Blood Flow and Metabolism*. <https://doi.org/10.1038/jcbfm.1984.42>

Wu, S., Avila-Sakar, A., Kim, J., Booth, D. S., Greenberg, C. H., Rossi, A., Liao, M., Li, X.,

Alian, A., Griner, S. L., Juge, N., Yu, Y., Mergel, C. M., Chaparro-Riggers, J., Strop, P.,  
Tampé, R., Edwards, R. H., Stroud, R. M., Craik, C. S., & Cheng, Y. (2012). Fabs enable  
single particle cryoEM studies of small proteins. *Structure*.

<https://doi.org/10.1016/j.str.2012.02.017>

Xie, Y., Chang, S., Zhao, C., Wang, F., Liu, S., Wang, J., Delpire, E., Ye, S., & Guo, J. (2020).

Structures and an activation mechanism of human potassium-chloride cotransporters.

*Science Advances*. <https://doi.org/10.1126/sciadv.abc5883>

Yang, X., Wang, Q. & Cao, E. Structure of the human cation–chloride cotransporter NKCC1

determined by single-particle electron cryo-microscopy. *Nat. Commun.* (2020)

[doi:10.1038/s41467-020-14790-3](https://doi.org/10.1038/s41467-020-14790-3).

Zeuthen, T. (1994). Cotransport of K<sup>+</sup>, Cl<sup>-</sup> and H<sub>2</sub>O by membrane proteins from choroid plexus

epithelium of *Necturus maculosus*. *The Journal of Physiology*.

<https://doi.org/10.1113/jphysiol.1994.sp020243>

Zhao, Y., Chen, S., Swensen, A. C., Qian, W. J., & Gouaux, E. (2019). Architecture and subunit

arrangement of native AMPA receptors elucidated by cryo-EM. *Science*.

<https://doi.org/10.1126/science.aaw8250>

Zhu, S., Noviello, C. M., Teng, J., Walsh, R. M., Kim, J. J., & Hibbs, R. E. (2018). Structure of a

human synaptic GABAA receptor. *Nature*. <https://doi.org/10.1038/s41586-018-0255-3>

Zhu, S., Stein, R. A., Yoshioka, C., Lee, C. H., Goehring, A., McHaourab, H. S., & Gouaux, E.

(2016). Mechanism of NMDA Receptor Inhibition and Activation. *Cell*.

<https://doi.org/10.1016/j.cell.2016.03.028>